1-1-1968

Turbulent mixing measurements for single phase air, single phase water, and two-phase air-water flows in adjacent rectangular subchannels.

Kenneth J. Petrunik
University of Windsor

NOTE TO USERS

TURBULENT MIXING MEASUREMENTS FOR SINGLE PHASE AIR, SINGLE PHASE WATER, AND TWO-PHASE AIR-WATER FLOWS IN ADJACENT RECTANGULAR SUBCHANNELS

by

KENNETH J. PETRUNIK

Submitted to the Faculty of Graduate Studies through the Department of Chemical Engineering in Partial Fulfilment of the Requirements for the Degree of Master of Applied Science at the University of Windsor

Windsor, Ontario

1968

ABJ 7251

APPROVED BY:

M B Powley

Robert A. Hagen

L. W. McDonald

C. St. Pierre

217505

ABSTRACT

Turbulent mixing* rates between two adjacent rectangular channels (0.80 in. x .74 in.) were measured for single phase air, single phase water, and two-phase air-water flows. Methane was employed as the air tracer and potassium nitrate (KNO_3) as the water tracer. A gas chromatograph and an atomic absorption unit were used for gas and liquid analyses respectively.

Single phase air turbulent mixing rates were determined at a system pressure of 50 psia using interconnection gaps 100 mils wide and 2,4,6,10,14 inches long. Also a 40 mil gap and 4 inch long interconnection path was used. The Reynold's number ranged from 15,000 - 150,000. In all cases the subchannel dividing strip was 0.125 inches thick.

Data for single phase water were taken at atmospheric pressure employing a gap of 100 mils and 4,10, and 14 inch long interconnection lengths. Reynold's numbers for single phase water flows were varied from 5000 to 30,000. The turbulent mixing data exhibited entrance effects similar to those previously observed in heat transfer under analogous conditions.

---

* Turbulent mixing is defined here as transfer of fluid between adjacent subchannels due to the random motion of turbulent flow.

Two-phase two-component turbulent mixing was studied for an air-water system with a gap of 100 mils and an interconnection-length 10 inches long. All data points were taken at a pressure of 50 psia. Quality was varied from 20% to 80% at four different mass fluxes. The percentages of air and water in a subchannel which mixed increased significantly as the quality* and mass flux decreased. It is postulated that the transitional flow regime from slug to annular flow and the presence of large roll waves give rise to this phenomena.

---

* Quality is defined here as the ratio of air mass flow rate to the total air and water mass flow rates.

AKNOWLEDGEMENTS

The author wishes to express his gratitude to Dr. C. St. Pierre for his assistance and advice in this study.

The experimental work for this thesis was performed at the Chalk River Nuclear Laboratories. Thanks are due to Mr. G.A. Wikhammer, Mr. S. Harris, Dr. D. McPherson, Dr. N. Sagert and Mr. A. Smith for their advice and assistance. Thanks are also due to Mr. O. Brudy, Mr. P. Liebsch and Mr. W. Wilke who constructed the test section used in this study.

The financial support provided by the National Research Council and Atomic Energy of Canada Limited is gratefully aknowledged.

TABLE OF CONTENTS

LIST OF FIGURES

LIST OF TABLES

I INTRODUCTION

The object of the present work was to measure the turbulent mixing rate between two adjacent interconnected rectangular subchannels* in which single phase air, single phase water, and two-phase air-water mixtures are flowing.

In the early design of heat exchange systems for Canadian nuclear reactors, experiments were performed on multi-rod bundles to determine the kinds and amount of interaction between interconnected subchannels. When one subchannel has a higher power factor than those adjoining, this can lead to critical heat flux conditions prematurely in this subchannel. However energy transfer by turbulent mixing from the hot channel to the colder channels gives rise to improved performance. Hence an accurate prediction of turbulent mixing will allow power reactors to be designed to operate at maximum thermal efficiency and economy.

There are two main classifications of interactions between adjacent subchannels. The first is generally given the name crossflow or diversion flow. Crossflow is defined as the net transfer of fluid from one subchannel to another when radial pressure gradients are the driving force. The second interaction phenomena is termed turbulent mixing. Turbulent mixing is the interchange of fluid between adjacent

---

* Subchannel is defined here as the flow area formed by drawing a line between the rod centres of a rod (tube) bundle heat exchanger. See Fig. 1.1.

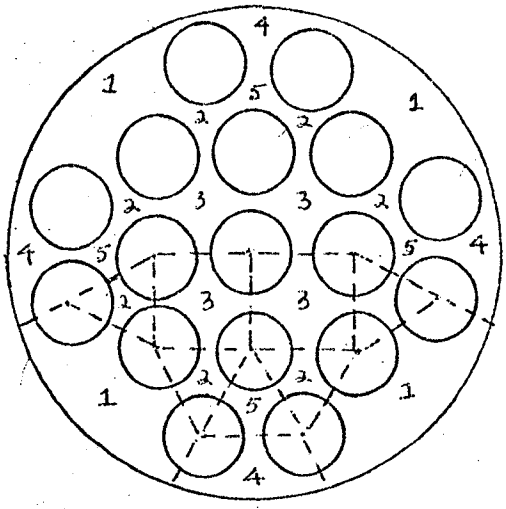

Total Number of Subchannels = 20

Total Number of Distinct Subchannels = 5

FIG. 1.1 Typical Rod Bundle Cross Section

subchannels due to the fluid flow turbulence. In this second type of interaction there is no net transfer of fluid between subchannels.

The effect of interconnection length and gap width on the degree of turbulent mixing for single phase air and single phase water were studied. In addition two-phase air-water mixing rates were measured as

a function of quality and mass flux.

In order to ensure that turbulent mixing measurements were not influenced by crossflow two conditions were maintained. First, equal pressure drops in each subchannel were obtained by use of upstream and downstream drag adjustments (when required). Secondly for each data point, mixing rates were measured for tracer being injected first into the left and then the right subchannel. If the values for left and right subchannel tracer injection differed by more than $\pm$ 10% indicating significant crossflow, then they were rejected and the run repeated.

The tracers used were methane for the gas phase and potassium nitrate for the water. Analyses of the methane air tracer were made on a gas chromatograph and the liquid phase tracer concentrations were determined by atomic absorption.

Since this was a basic study of turbulent mixing, the simplest subchannel array was chosen. See Fig. 1.2. It consisted of two rectangular channels formed by a 1/8 inch dividing strip which had cut in it slits of various lengths and widths (gaps).

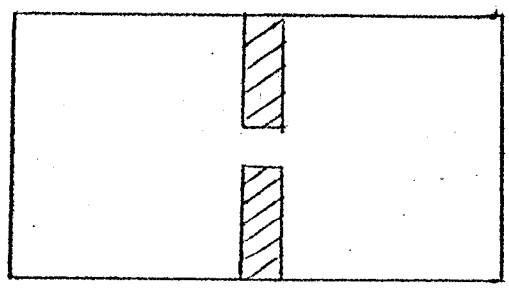

Fig. 1.2
Subchannel
Cross-section

II LITERATURE SURVEY

A. Introduction

An excellent discussion of turbulent mixing and available correlations has been given by Rogers and Todreas [1]. Rogers and Todreas defined two new types of mixing: flow scattering and flow sweeping. Flow scattering is due to the presence of rod spacers and fuel bundle end plate assemblies which induce turbulence. This phenomena is said to be non directional. Flow sweeping has a directional flow effect caused by wire wrap spacers, helical fins, etc. This is essentially a crossflow phenomena since it results in a net transfer of fluid from one subchannel to another.

Turbulent mixing (without any turbulence promoters) results from the random motion of macroscopic portions of the fluid stream flowing under turbulent flow conditions. Heat and mass transfer data for systems in turbulent flow are often correlated using the concept of turbulent or eddy diffusivities for heat or mass. Because of the nature of turbulent flow there is an increase in the transport properties of the fluid and molecular diffusion becomes negligible compared to turbulent diffusion. The equations for heat and mass transfer can be written as follows:

Molecular

heat $$Q = -(k/\rho C_p)(\nabla \rho C_p T) \qquad (2.1)$$

mass $$J_A = -D\nabla C \qquad (2.2)$$

Turbulent

$$\text{heat} \quad Q = -(k/\rho C_p + E_H)\nabla \rho C_p T \simeq -E_H \nabla \rho C_p T \qquad (2.3)$$

$$\text{mass} \quad J_A = -(D + E_m)\nabla C \simeq -E_m \nabla C \qquad (2.4)$$

where

C	= concentration	lbm/ft^3
C_p	= heat capacity	$BTU/lb\,^oF$
D	= molecular diffusivity	ft^2/hr
E_H	= eddy diffusivity (heat)	ft^2/hr
E_m	= eddy diffusivity (mass)	ft^2/hr
J_A	= mass flux of A	$lb/hr\ ft^2$
k	= thermal conductivity	$BTU/hr\ ft^2\ ^oF/ft$
Q	= heat flux	$BTU/hr\ ft^2$
T	= temperature	^oF
ρ	= density	lb/ft^3

The eddy diffusivities for heat and mass have been found to be equal [1,2,3]. Mass diffusion studies have been used to predict turbulent heat transfer rates.

B. Single Channel Experiments

There are two basic approaches in the experimental determination of turbulent (eddy) diffusivities. The first involves the addition of tracers (or heat) into a fluid stream and subsequent concentration (or temperature) measurements downstream. Wilson[4] integrated the steady state Fourier heat conduction equation for the continuous addition of heat from a point source in an infinite fluid stream moving at a uniform velocity in one direction. Measurements of

axial or radial temperature (concentration) profiles used in conjunction with Wilson's solution enables the determination of the turbulent diffusivities for heat (mass) transfer. This approach was used by Towle and Sherwood [5], Slember [6], McCarter, Stutzman and Koch [7], and Pfennigworth and Steer [8].

An alternate approach is to measure eddy diffusivities by determining the rate of water transfer from a liquid film (viz. wetted wall column) as done by Sherwood and Woertz [9] and Dhanack [10].

Most of the available data has been correlated by St. Pierre[11] and plotted as ψ versus N_{Re}, where ψ is the inverse of the Peclet number. This represents the ratio of turbulent conductive mass transfer to bulk mass transfer ($\psi = \frac{E}{\langle V \rangle De}$).

The major problem with this approach lies in the fact that the values of turbulent diffusivities obtained are for the case of a single channel. For subchannel analysis they must be applied to the region between subchannels and for different rod cluster geometries. An order of magnitude value for turbulent mixing between subchannels can be determined employing eddy diffusivities from the above methods but it is not sufficiently accurate to meet present requirements for a rigorous subchannel analysis.

C. Multi-Channel (Rod Bundle) Experiments

Tracer experiments have been carried out in multirod bundles to determine flow interchange between subchannels. It is important to note that in this type of analysis some crossflow effects may also be present. The total flow redistribution from all effects is measured.

A tracer (hot water, salt, dye, gas) is injected in one subchannel and concentrations measured in adjacent channels downstream to determine the rate of flow interchange. A tracer mass balance is used to calculate a mixing coefficient.

Rogers [12] has employed rod bundle mixing data and proposed a correlation for single phase fluid interchange for rod bundles. Taking an energy balance between the heat transport rate by the postulated mixing flow and the radial heat transport by eddy diffusivity between any two channels i and j he develops a relationship for flow mixing between adjacent subchannels:

$$\omega^t C_p(\overline{T}_i - \overline{T}_j) = \rho C_p b L E_{ij} \left(\frac{d\overline{T}}{dr}\right) \tag{2.5}$$

By writing the mean temperature gadient as $(\overline{T}_i - \overline{T}_j)/Z_{ij}$ where Z_{ij} is an intersubchannel distance equation (2.5) can be rewritten as:

$$\frac{\omega^t}{L} = \frac{\rho\, b\, E_{ij}}{Z_{ij}} \tag{2.6}$$

This form of equation is analogous to those proposed by St. Pierre [11], Bowring [13] and Rowe and Angle [14].

St. Pierre

$$\frac{\omega^t}{L} = \frac{\rho b E}{1/2\,(R_{eq_i} + R_{eq_j})} \tag{2.7}$$

Bowring

$$\frac{\omega^t}{L} = \frac{F_m}{S_m}\,\frac{b}{d}\,E\,\rho \tag{2.8}$$

Rowe and Angle

$$\omega^t = \frac{\rho b E}{\Delta y} \tag{2.9}$$

where

ω^t	= mixing rate	lb/hr
ρ	= density	lb/ft^3
b	= gap width	ft
d	= rod diameter	ft
R_{eq}	= 1/2 equivalent diameter	ft
E	= eddy diffusivity	ft^2/hr
Δy	= gap width (in correlation)	ft
S_m	= gap shape factor	-
F_m	= emperical mixing factor to account for turbulence promoters	-

It is evident that the above equations are identical in form differing only in the definition of an intersubchannel distance.

Rogers [12] postulates that Z_{ij} is a function of (b/d) and using the data of Clarke [15], Tarasuk and Kempe [16], Collins and France [17], Bishop [18], Nelson [19], Dean [20], Biggs and Rust [21] has developed an empirical correlation which predicts mixing as a function of (b/d). Rogers correlation predicts a constant mixing rate for $.05 < b/d < .5$ since both Z_{ij} and E_{ij} decrease at the same rate as (b/d) decrease. For $b/d < .05$ there was an increase in mixing rate with decreasing b/d. This correlation would suggest that single channel diffusivities cannot be applied to rod bundles since E is a function of b/d. The next approach followed in mixing experiments between adjacent subchannels is that in which both subchannels are pressure balanced to eliminate radial pressure gradients and hence crossflow.

D. Two Channel Experiments

1. Singleton [22]

Limited data have been obtained for single phase turbulent mixing between similar adjacent subchannels. Singleton measured water mixing rates between adjacent subchannels using a dye as a tracer. His subchannel arrangements are detailed in Fig. 2.1. For the square fillers at the same Reynold's number the mixing rate increase was approximately 1.4 times that given by the ratio of the gap widths. For the round fillers at the same Reynold's number the mixing rate increase was approximately proportional to the ratio of the gap widths. Mixing is increasing with gap width but the mixing for the square filler increased more than the gap width ratio. The cause is not readily explainable. Singleton evaluated his data in terms of a mixing coefficient and his data were reanalyzed in terms of an equivalent Stanton number for purpose of comparison here. (See Appendix III).

2. Rowe and Angle [23,24]

Rowe and Angle have obtained turbulent mixing data between adjacent triangular-rectangular subchannels by measuring the enthalpy rise in a heated test section. Their equation for mixing was obtained by using their computer code [14] to determine a Stanton number which most closely matched their experimental results. Three data points were obtained for $(b/d) = 0.0355$ and eight data points for $(b/d) = 0.149$. Their correlation predicts the mixing rate to be independent of rod spacing.

Data were taken also for a square-square subchannel array (Fig. 2.1) using lithium hydroxide as a tracer. Here their computer

All dimensions are given in inches

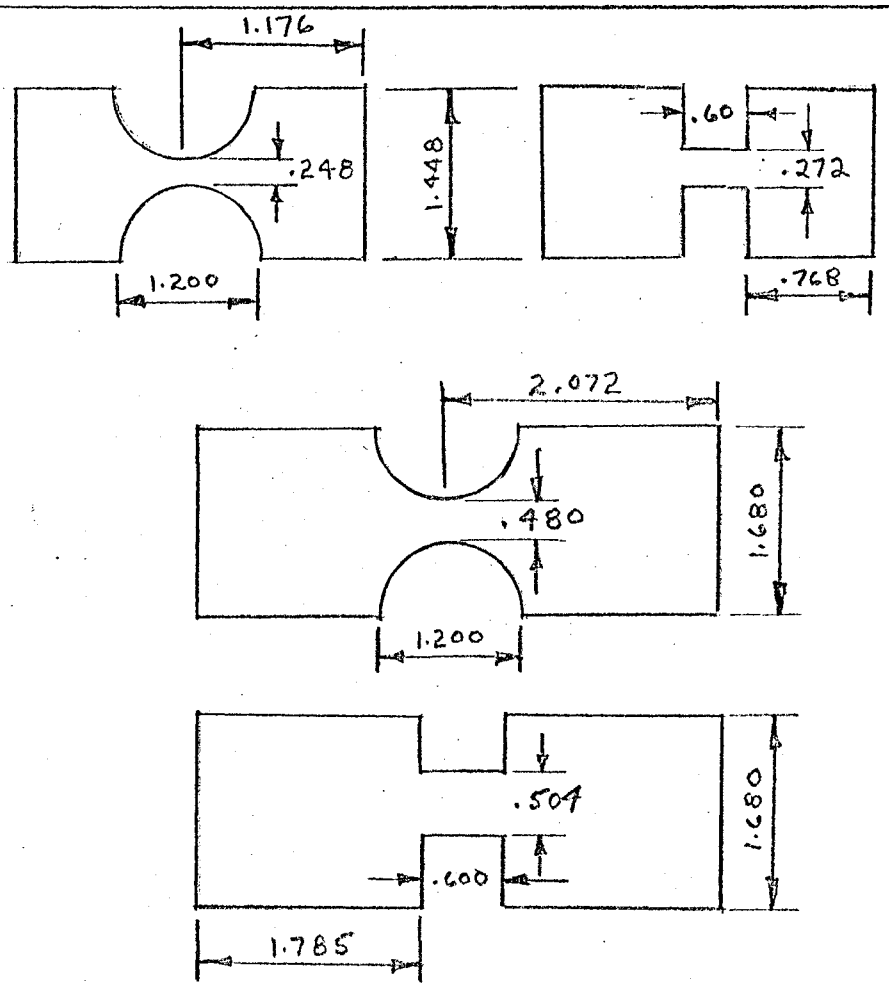

Singletons Subchannel Dimensions

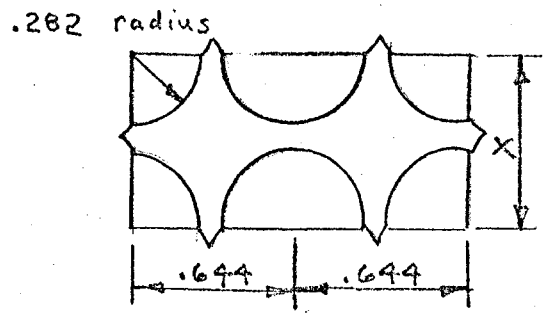

Gap width	.020	.085
X	.584	.644

Rowe and Angle Subchannel Dimensions

FIG. 2.1

Subchannel Details of Singleton and Rowe and Angle

code yielded a correlation which predicted that the mixing rate was again independent of (b/d).

Mixing for the square square array was less than for the square triangular array. Hence mixing decreased as the centroidal distance between two subchannels increased.

Further experimental data are necessary for single phase mixing as there is presently insufficient data to predict turbulent mixing rates for all types of subchannels and all ratios of gap width to rod diameter.

E. Single Phase Turbulent Mixing Correlations

1. St. Pierre Correlation [11]

St. Pierre has proposed a correlation for turbulent mixing rates based on values of turbulent diffusivities obtained from single channel experiments.

$$\frac{\omega^t}{L} = \frac{b\rho E}{1/2\ (R_{eqi} + R_{eqj})} = 2bG\psi \qquad (2.10)$$

where

$$\psi = .0205\ N_{Re}^{0.0205} \qquad N_{Re} > 5000.$$

2. Bowring Correlation [13]

Bowring has developed a subchannel code Hambo in which the following single phase mixing equation is used.

$$\frac{\omega^t}{L} = \frac{Fm}{Sm}\frac{b}{d} E\ \rho$$

$$= Fm\ \frac{b}{d}\ Sm \quad \frac{f_i + f_j}{80}\ (D_i G_i + D_j G_j) \qquad (2.11)$$

Assuming equal subchannels and Fm = 1.

$$\frac{\omega^t}{L} = \frac{b}{\bar{d}S_m} (.215\ N_{Re}^{-.1})\ DG. \tag{2.12}$$

3. Rogers and Tarasuk Correlation [12]

Using the experimental data outlined previously Rogers and Tarasuk have developed a correlation from multi-channel experiments.

$$N_{st} = \frac{k}{2} (b/\bar{d})^{-r} N_{Re}^{m-1} \left(1+\frac{De_j}{De_i}\frac{3m}{2-n}\right) \frac{De}{\bar{d}} \tag{2.13}$$

Values of m,n,k, and r were obtained from an analysis of the experimental data. Considering two similar adjacent subchannels the above expression reduced to:

$$N_{st} = \frac{.0503}{2} (b/\bar{d})^{-1.57} N_{Re}^{-.32} (1+1) \frac{De}{\bar{d}} \tag{2.14}$$

or Roger's correlation No. 1:

$$\frac{\omega^t}{L} = .0503\ (\bar{d}/b)^{.57}\ De\ G\ N_{Re}^{-.32} \tag{2.15}$$

Rogers [25] has modified the above correlation to account for the difference in subchannel arrays. A tentative equation (Roger's correlation No.2) has been proposed as:

$$\frac{\omega^t}{L} = .050\ D_e\ G\ N_{Re}^{-.32} \tag{2.16}$$

Additional data and reanalysis [25] have shown that the correlation for similar subchannels reduces to a form identical with that of Rowe and Angles correlation. The only difference lies in the constant being 0.0035 for Roger's and 0.0036 for Rowe and Angle. In this reanalysis Rogers shows that mixing rates from rod bundle experiments are approximately 2.3 times that of subchannel experiments.

4. Rowe and Angle Correlation [23,24]

The Rowe and Angle correlation was developed by finding a value of the equivalent Stanton number which most closely matched their experimental data.

$$Nst = Kr \left(\frac{De}{Z_{ij}}\right) N_{Re}^{-n/2} \tag{2.17}$$

where

Kr = .0062 triangular-square array

Kr = .0036 square-square array

n = .2

Z_{ij} = b(gap width)

With the above values for the constant Eq. (2.17) reduces to:

$$\frac{\omega^t}{L} = Kr \frac{De}{b} G N_{Re}^{-.1} \tag{2.18}$$

5. Moyer Correlation [26]

Moyer has proposed the following correlation for turbulent mixing:

$$\frac{\omega^t}{L} = \frac{(2a)^{1/2}}{40} \frac{De}{Z_{ij}} b G N_{Re}^{-n/2} \tag{2.19}$$

where:

n = .2

a = .0405 i.e. $f = a N_{Re}^{-n}$

Z_{ij} = centroidal distance between subchannels

$$\frac{\omega^t}{L} = .0255 \frac{De}{Z_{ij}} b G N_{Re}^{-.1} \tag{2.20}$$

F. Two Phase Turbulent Mixing Data

Experimental data for two phase turbulent mixing are very limited. Bestenbreuer and Spight [27] have injected air in one subchannel and measured the mass flow of air and water at the outlet of the channels.

Rowe and Angle [23,24] have obtained experimental data on two phase steam water turbulent mixing at elevated pressures. The first experiments were carried out using a triangular-rectangular subchannel array. Their data were analyzed and a mixing coefficient β (which is equivalent to N_{st}) obtained from an enthalpy balance on their heated test section using their computer code. The results are summarized below in Table 2.1.

TABLE 2.1

Two-Phase Mixing Data of Rowe and Angle Triangular-Square Array

b	6×10^{-6}	β	β	Boiling Mixing
inches	lb/hr ft^2	non-boiling	boiling	Increase %
.084	1	.006	.024	300
.084	2	.006	.012	100
.084	3	.006	.012	100
.020	2	.020	.020	0
.020	3	.020	.020	0

Further experiments were carried out with a square-square subchannel array using lithium hydroxide as the liquid tracer and deuterium and tritium as total tracers since the proportion of the latter two is about equal for liquid and vapour. Their results showed that a maximum value of mixing was reached at low qualities and that the percent mixing

increased with increasing mass flux. The ratio of steam to water mixing was found to be equal to the ratio of the total steam flow to the total water flow.

III THEORY

A. Derivation of Mixing Equation

Consider a fluid passing under turbulent flow conditions through two identical parallel channels interconnected through a gap parallel to the flow direction. Since turbulent flow is characterized by random fluctuations in the fluid velocity, movement of macroscopic portions of the fluid stream gives rise to a phenomena known as turbulent mixing. Turbulent mixing does not result in a net transfer of fluid between interconnected subchannels. Small masses of fluid move from one channel to the other but the total flow in each channel remains the same.

In order to determine the amount of mixing taking place, a tracer is injected into one subchannel and an equal mass of fluid in the other subchannel so that the subchannel flows remain equal. Measurements of the tracer concentrations in each subchannel can then be used to determine the degree of turbulent mixing.

Basic Assumptions:

(1) The total flow of fluid plus tracer is identical in each subchannel.

(2) The geometry of each subchannel is identical. Hence the axial pressure gradients are identical and no radial pressure gradients exist.

(3) The tracer concentration is small and has no effect on the flow properties of the carrier fluid.

(4) Fluid moving from one subchannel to the other is assumed to have the average properties (concentration of tracer) of the channel which it is leaving. Also, when a small mass of fluid enters a subchannel it mixes quickly with the fluid in that channel.

Consider a tracer mass balance on subchannel 1 in the following figure.

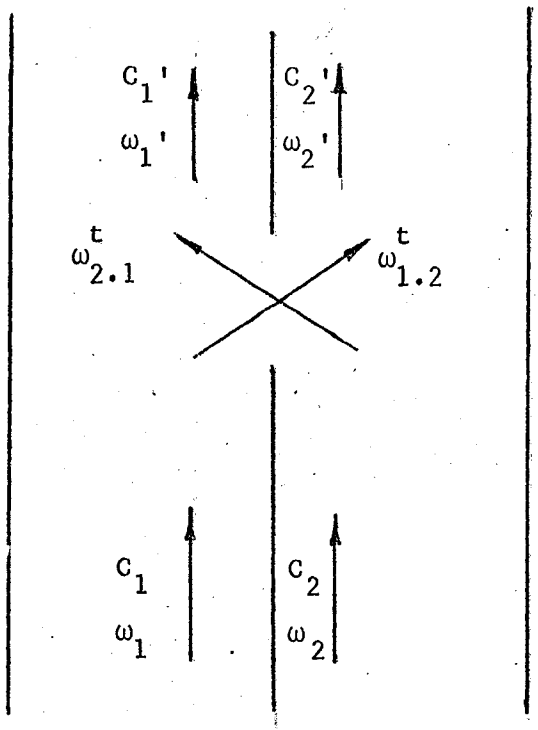

Fig. 3.1 Mixing Flow Diagram

$$\omega_1 C_1 + \omega^t \left(\frac{C_2' + C_2}{2}\right) - \omega^t \left(\frac{C_1' + C_1}{2}\right) = \omega_1' C_1' \qquad (3.1)$$

Assume that the tracer is injected in channel 1. Therefore $C_2 = 0$ and noting that $\omega_1 = \omega_2 = \omega_1' = \omega_2'$:

$$\omega(C_1 - C_1') = \frac{\omega^t}{2}(C_1' + C_1 - C_2') \qquad (3.2)$$

From an overall tracer balance:

$$C_1 = C_1' + C_2' \tag{3.3}$$

Substituting Eq. (3.3) in (3.2)

$$\omega C_2' = \frac{\omega^t}{2} (C_1' + C_1' + C_2' - C_2') \tag{3.4}$$

which reduces to:

$$\omega^t = \omega\left(\frac{C_2'}{C_1'}\right) \tag{3.5}$$

As long as $C_1 \approx C_1'$ employing the arithmetic mean for subchannel concentrations should be valid.

Mixing can also be determined using a differential tracer balance on subchannel 1. Expressing the concentrations as relative concentrations i.e. $C_1^* + C_2^* = 1$ the differential tracer balance can be written as

$$\omega_2 C_2^* + \omega^t C_1^* \, dx - \omega^t C_2^* \, dx = \omega_2 C_2^* - \omega dC_2^* \tag{3.6}$$

This reduces to

$$\frac{dC_2^*}{dx} = \frac{\omega^t (C_1^* - C_2^*)}{\omega} \tag{3.7}$$

Since $C_1^* + C_2^* = 1$ Eq. (3.7) becomes

$$\frac{dC_2^*}{dx} = \frac{\omega^t}{\omega} (1 - 2 C_1^*) \tag{3.8}$$

This can be solved to give

$$\frac{C_2'}{C_1} = 1/2 \left[1 - \exp\left(-\frac{2\omega^t L}{\omega}\right)\right] \tag{3.9}$$

There was no difference between the calculated values of ω^t employing Eq. (3.5) and Eq. (3.9) in this analysis.

B. Discussion of Flow Regimes

Two phase mixing is expected to be a strong function of flow regime. Basically there are four main two-phase flow patterns along with transition regions between them. These are bubble flow, slug flow, annular flow and mist flow (Fig. 3.2). In bubble flow the liquid is the continuous phase with the vapour bubbles as the discontinuous phase. As the number of bubbles increases (increasing quality) they coalesce to form long slug like bubbles. As the quality increases further the slugs break down to form an annular flow. This is characterized by a film of liquid on the channel wall and entrained liquid in the core of the channel. Finally increasing the quality still further, more of the liquid is stripped from the wall and entrained in the core. This is known as fog or mist flow. The prediction of the transition between regimes is important in order to predict two-phase turbulent mixing rates.

A correlation for predicting the transition regime from slug to annular is given by Wallis [28]. Criteria for annular flow are presented in terms of j_g^* and j_l^* which are dimensionless gas and liquid velocities. The data are plotted in Fig. (3.3). All the data taken here lie in the annular flow regime or fog flow regime.

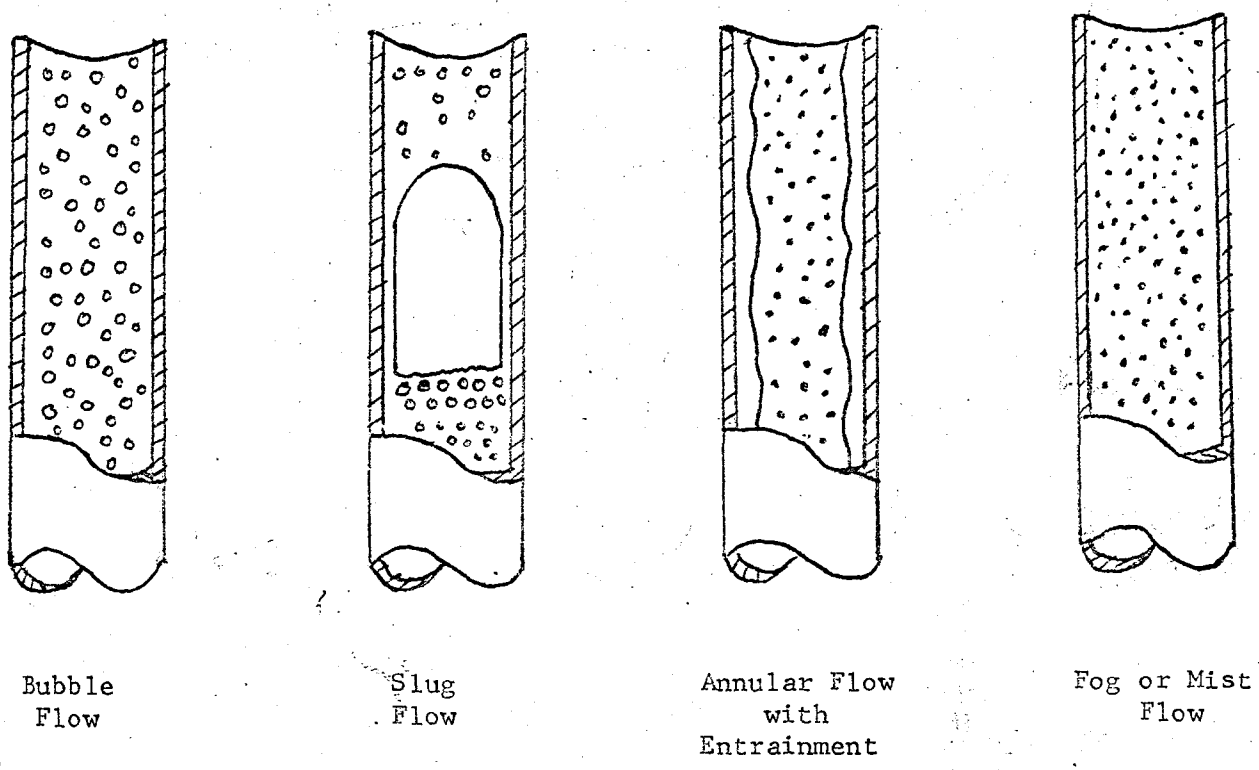

FIG. 3.2 Illustration of Two-Phase Flow Patterns

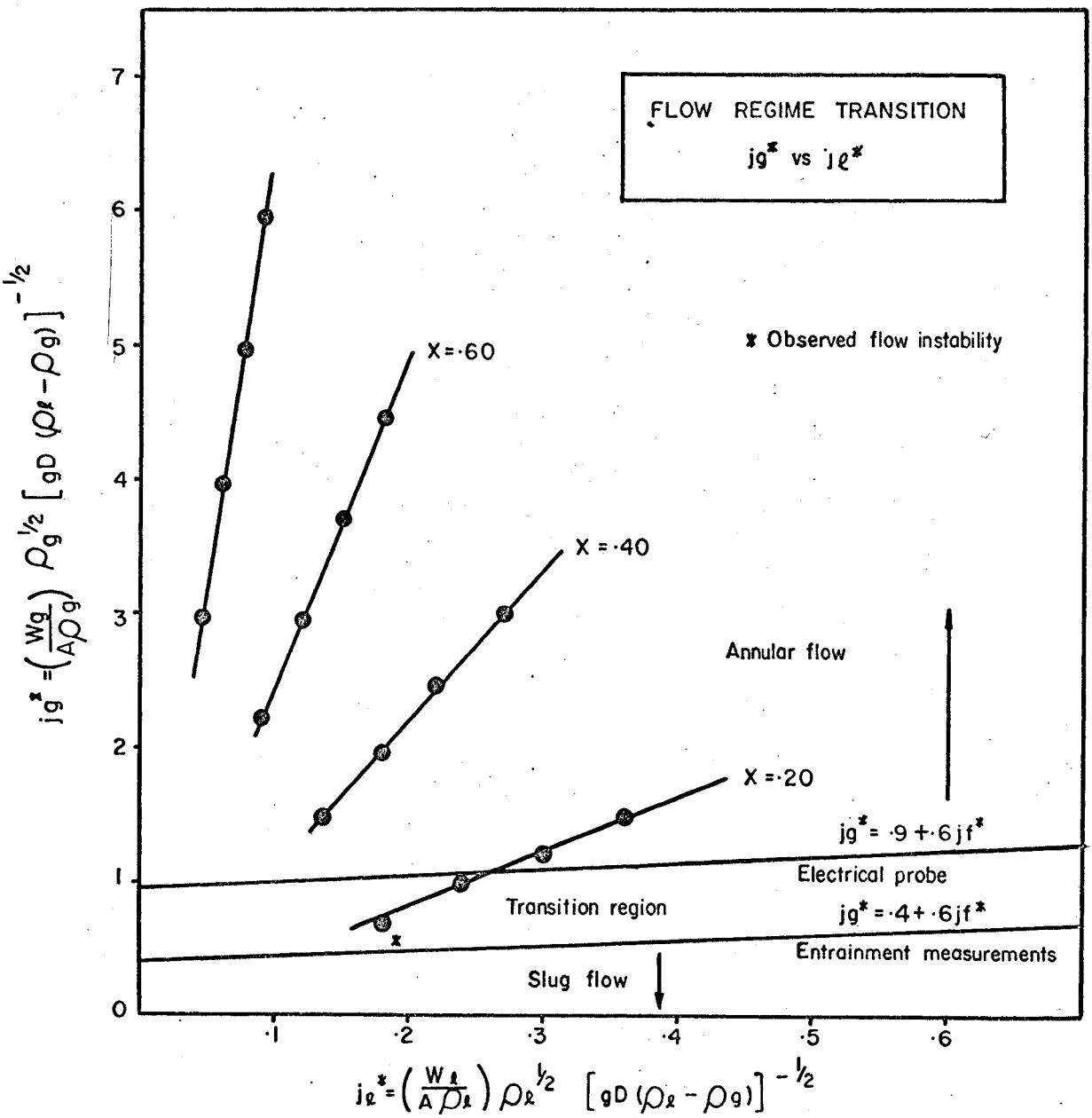

FIG. 3.3

Flow Regime Transition Map of Wallis [28]

IV AIR-WATER TEST LOOP AND ASSOCIATED EQUIPMENT

A. Experimental Equipment

1. Air-Water Test Loop

The air-water test loop WAFER* and associated equipment used in this study were located in the Advance Engineering Building at Chalk River Nuclear Laboratories. Initially this loop was designed and constructed [29] to permit two-phase flow studies on prototype nuclear reactor rod bundle geometries. For the purposes of this mixing experiment minor modifications were made to the loop.

The air-water test loop used in this study consisted essentially of a regulated 100 psig air supply, a centrifugal pump for water circulation, an orifice metering system, a test section assembly, and a cyclone separator.

The loop is diagrammed schematically in Fig. 4.1.

Air from a 100 psig. air service line of the plant was filtered and metered through a bank of four orifices to the mixer. An air vent valve on the separator was employed to maintain a constant test section pressure at the beginning of the interconnection length for all experimental runs.

Water was supplied by a Durco (Model H7RDR4) centrifugal pump which could provide 100 IGPM at a head of 107 psia.

---

* Water Air Fog Experimental Rig located at Chalk River Nuclear Laboratories (Building 456).

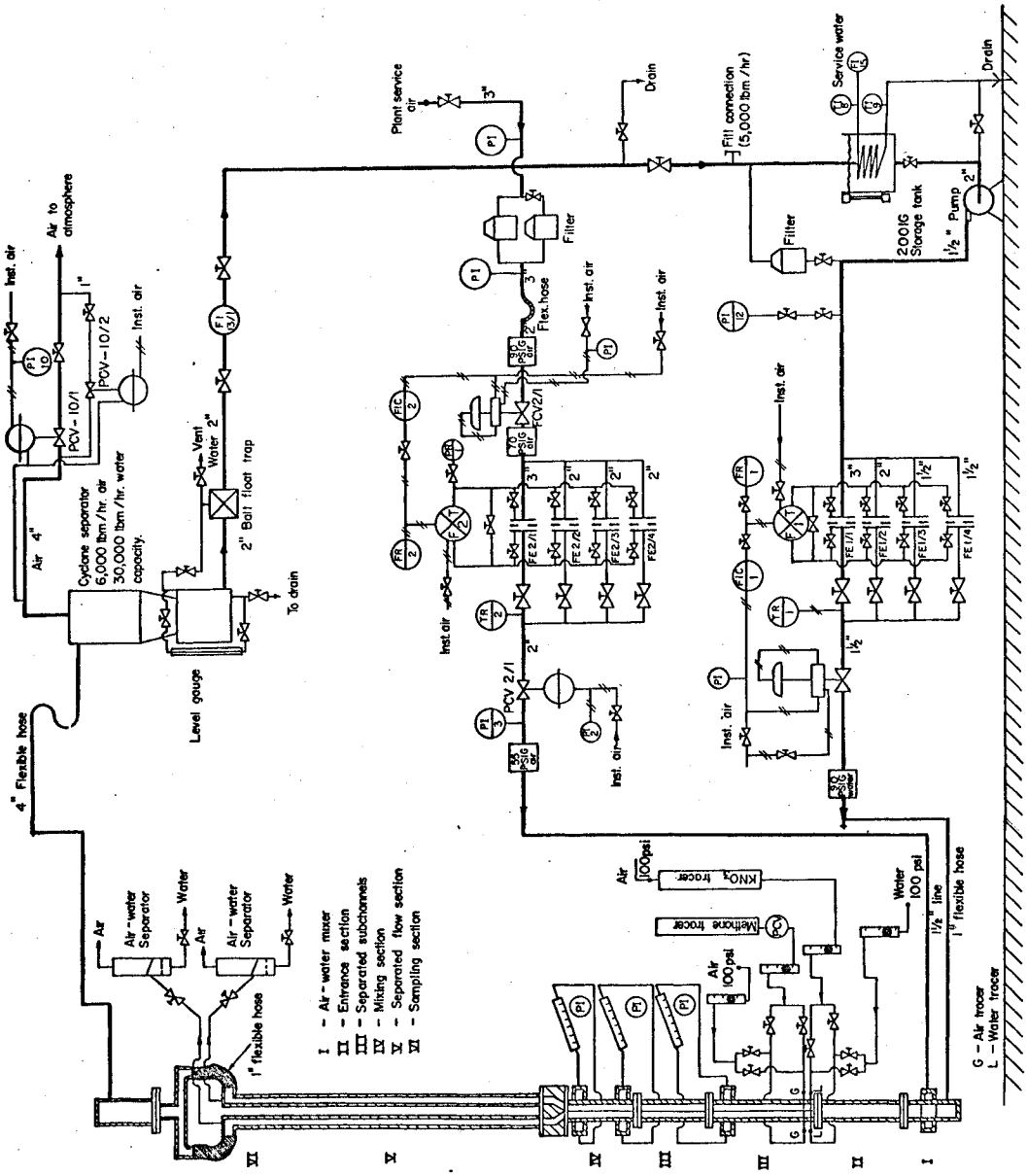

FIG. 4.1 Schematic Flow Diagram of WAFER

A bank of four orifice meters was employed to meter the water flows before entering the mixer. In addition a flowmeter with 1200 lbm/hr capacity was placed in parallel with the four water orifices to measure the low water flow rates.

After the test section assembly, a cyclone separator with a capacity of 6000 lbm/hr of air and 30,000 lbm/hr of water was used to separate the water from the air. The air leaving the separator passed through a pressure control valve and then was vented to the atmosphere. The water passed through a 2-inch ball float trap to a downcomer. It then could be sent to a drain or recycled to a 200 IG. feed storage tank. In order to avoid tracer contamination the loop was operated on a once-through basis.

2. Test Section Assembly

The test section assembly consisted of six sections: I - air-water mixer, II - entrance section, III - separated subchannels, IV - interconnected subchannels, V - separated flow channels, VI - sampling section. A detailed drawing of the test section assembly is given in Fig. 4.2. The test section was fabricated entirely from acrylic to allow visual identification of the flow regimes. The various sections were butted together using 0.005 inch thick natural rubber gaskets cut to fit the channel shape.

(a) Mixer Section.

The air-water mixer consisted of an annular ring surrounding the rectangular channel at the test section entrance. Six 3/8 inch holes through which the water passed were drilled in the channel wall.

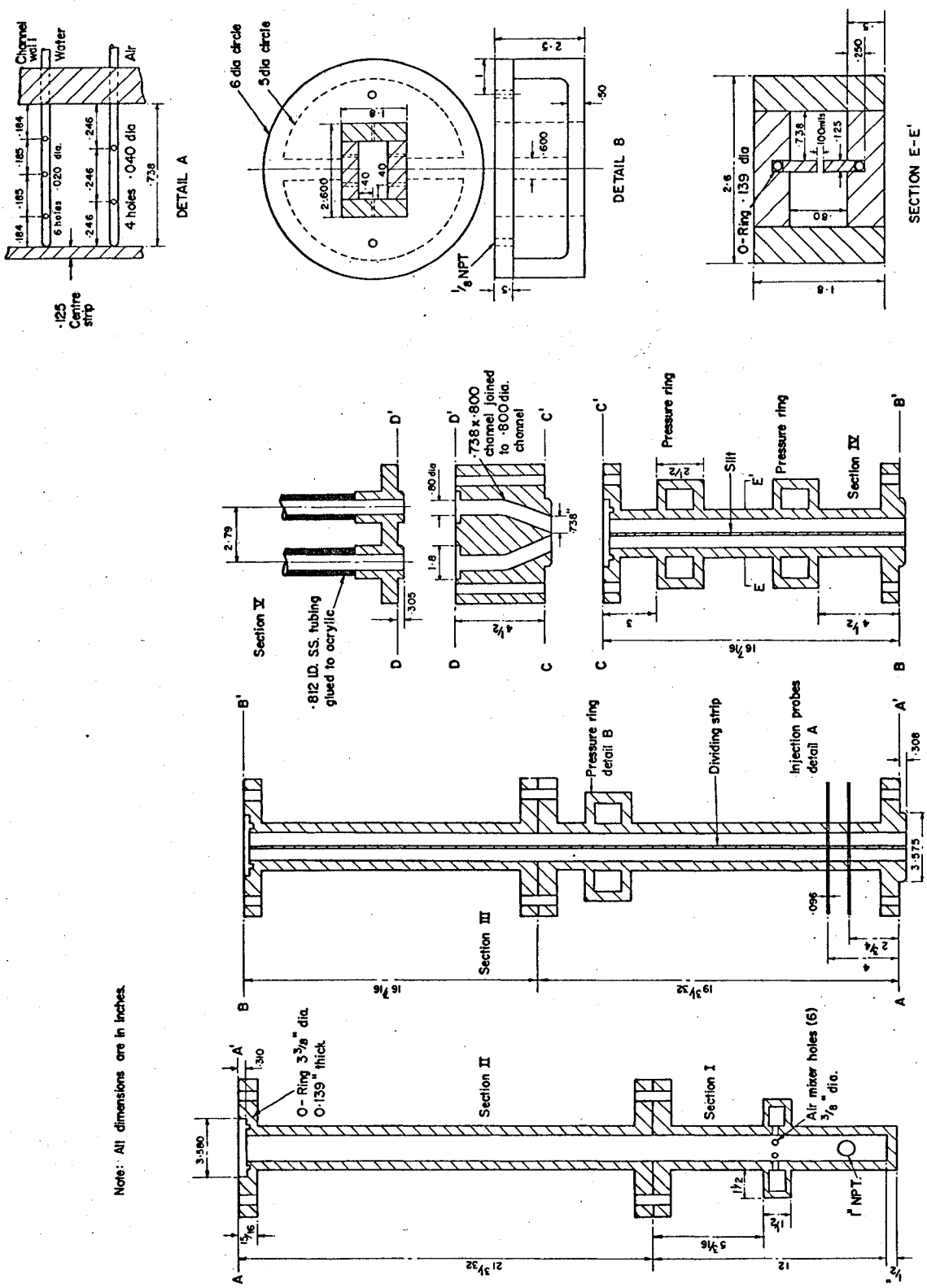

FIG. 4.2

TEST SECTION ASSEMBLY

217503

The air passed directly into the rectangular test section.

(b) Entrance Section.

The 22 inch entrance section was located after the mixer to allow the flow to develop before being split into two subchannels.

(c) Separated Subchannels.

The rectangular flow area was split here into two subchannels 36-13/22 long by means of a 1/8 inch dividing strip. The downstream edge of the dividing strip was in the form of a knife edge to reduce flow turbulence. Injection probes for the air and water tracers were located just after the flow was split. The probes are detailed in Fig. 4.2.

(d) Interconnected Subchannels.

Mixing occurred in this 16-7/16 inch section through the gap in the dividing strip. An O-ring seal was employed around the dividing strip to facilitate removal when changing the interconnection dimensions.

(e) Separated Channels.

The subchannel flows were separated here and entered seven foot long 0.812 inch stainless steel tubes. This was done to ensure adequate mixing of tracer.

(f) Sampling Section.

A portion of the total flow was taken from each of the stainless steel tubes and passed continuously to a small air-water separator. The bulk flow went to an air-water separator where the water removed was sent to the drain and air vented to atmosphere. The air exit line contained a back pressure valve which was used to control the

test section pressure. Air samples were collected in glass sampling tubes with stopcocks at each end. The water samples were collected in polyethylene bottles for later analysis.

B. Measurement of Loop Variables

1. Pressure Measurements

Three pressure rings were used to measure the radial pressure gradients which would cause crossflow. Each ring was constructed of two halves which were completely separated. Three static pressure taps were drilled from each half into the channel. See Fig. 4.2 for details.

The static pressure at the beginning of the subchannel interconnection length was maintained at 50 psia by means of a manual pressure control valve on the air outlet line of the separator. The axial pressure drop was measured employing the first two pressure rings. Radial pressure gradients were measured employing inclined manometers graduated to hundredths of an inch of water.

2. Flow Measurements

(a) Air

An automatic control loop maintained a constant test section flow. Four orifices were used as the primary flow measurement devices in conjunction with one differential pressure transmitter.

The orifices and assemblies conformed to ASME specifications [30] and were calibrated for the four following ranges detailed in Table 4.1.

TABLE 4.1

Air Orifice Specifications

Fig. 4.1 Designation	Orifice Diameter (in.)	Range (lbm/hr)
FE - 2/1	1.941	1700 - 6000
FE - 2/2	1.087	500 - 1800
FE - 2/3	0.6455	160 - 600
FE - 2/4	0.3540	40 - 180

(b) Water

Water flow rates to the test section were automatically controlled over the range 500 to 50,000 lbm/hr at loop operating pressures up to 100 psig. Four orifices meeting ASME specifications were also used in conjunction with one differential pressure tranducer to meter the water flows to the test section. (See Table 4.2). All orifices were calibrated over this temperature range 45°F to 100°F.

TABLE 4.2

Water Orifices

Fig. 4.1 Designation	Orifice Diameter (in.)	Range (lbm/hr)
FE - 1/1	1.665	12,000 - 50,000
FE - 1/2	0.9255	4,000 - 15,000
FE - 1/3	0.5400	1,400 - 5,000
FE - 1/4	0.2960	500 - 1500

3. Temperature

The temperature of both the air and water flow streams was measured using liquid filled thermocouple wells in the flow lines immediately after the orifice banks.

4. Tracer Concentrations

(a) Potassium Nitrate Analysis

Potassium nitrate (Anachemia purified) was used to make up the liquid tracer solution. Air pressure at 100 psig. over the potassium nitrate reservoir was used to force the tracer into the test section.

Potassium concentrations were measured using a Perkin Elmer 290 B atomic absorption analyzer with a hollow cathode potassium lamp. The atomic absorption analyzer was calibrated before each analysis over the working concentration range of zero to ten parts per million. Samples were diluted to fall into this range. Analyses were reproducible to $\pm$ 1.5 %.

(b) Methane Analysis

The methane tracer was supplied from gas cylinders (Matheson technical grade). The air samples taken in the glass sampling tubes were injected into a gas chromatograph with Porapak Q column and hydrogen flame detector. Daily calibration curves were made on the gas chromatograph. Analyses were reproducible to $\pm$ 1%.

V EXPERIMENTAL PROCEDURE

For all experimental mixing rate runs, single phase air, single phase water, and two-phase air-water mixtures, the tracers were injected alternately in each channel. If equal values of the mixing rate were measured for injection in each subchannel then crossflow effects were assumed to be absent. Both channels were pressure balanced employing, if necessary, a clamp on the flexible hose connection at each subchannel exit to alter the hydraulic resistance. For some of the higher mass fluxes a drag screw located just after the injection probles was also used. The channels were balanced to $\pm$ 6/100 inches water for single phase air runs and $\pm$ 1/10 of an inch of water for the two-phase air-water runs. In the single phase water runs the total head was measured at each piezometric ring in both subchannels. There was no measurable radial pressure gradient.

The flow split was checked by leaving the methane tracer flowmeter at a given reading and injecting into each subchannel. The concentrations measured had a maximum deviation of 3%. Since equal amounts of tracer were injected in each subchannel, tracer concentrations are proportional to the total flow. Therefore subchannel flow rates were always within 3% of each other.

The range of experimental parameters employed here is shown in Tables 5.1, 5.2, and 5.3.

TABLE 5.1

Single Phase Air Parameter Range

Pressure at beginning of interconnection length		50 psia					
Interconnection Details	gap mils	100	100	40	100	100	100
	length in.	2	4	4	6	10	14
Reynolds number, N_{Re}		15,000 - 150,000					
Total Mass Flux, G, lb/hr ft^2		$1 \times 10^4 - 1 \times 10^5$					

TABLE 5.2

Single Phase Water Parameter Range

Pressure at beginning of interconnection length		14.7 psia		
Interconnection Details	gap mils	40	100	100
	length in.	4	10	14
Reynolds number, N_{Re}		5,000 - 30,000		
Total Mass Flux, G, lb/hr ft^2		$2 \times 10^5 - 2 \times 10^6$		

TABLE 5.3

Two-Phase Air-Water Mixture

Pressure at beginning of interconnection length		50 psia
Interconnection Details	gap mils	100
	length in.	10
Total Mass Flux, G, lb/hr ft^2		$0.735 \times 10^5 - 1.46 \times 10^5$
Quality		0.2, 0.4, 0.6, 0.8

An important part of the experiment was the method of tracer injection. As a result it was decided to use four and six hole injection probes to insure a uniform tracer distribution. The injection method was checked by using a dye tracer. For single phase water runs the tracer distribution appeared homogeneous within 2 inches of the injection point. For two phase runs the tracer distribution appeared homogeneous within 4 inches of the injection point. The use of the small holes in the probes caused the liquid to emerge as an expanding jet which extended to the walls of the subchannel. This insured that for two-phase runs the tracer was present both on the walls and in the core of the channel.

In order to assess the amount of methane tracer which would be dissolved in the water a calculation was employed using the non-injection subchannel, since a significant degree of solubility would greatly affect the data. (See Appendix V). For the maximum water flow rate the amount of methane dissolved was of the order of 0.005%.

VI RESULTS AND DISCUSSIONS

Turbulent mixing rates between two adjacent rectangular subchannels are reported for single phase air, single phase water, and two-phase air-water mixtures.

A. Single Phase Data

One approach in the correlation of turbulent mixing rates comes from that originally proposed for single channel experiments. Here a dimensionless variable Ψ (the inverse of the Peclet number) is used to obtain a correlation in terms of a diffusivity. In this approach a distance term must be employed (as in the proposed equations 2.7, 2.8 and 2.9) in order to predict turbulent mixing rates.

A second approach in the correlation of mixing rate data involves the use of an equivalent Stanton number, N_{st}. For heat transfer the Stanton number is defined as:

$$N_{st} = \frac{h}{C_p G} = \frac{N_{Nu}}{N_{Re} N_{Pr}} = \frac{\text{heat actually transferred}}{\text{total heat capacity of fluid}}$$

For mass transfer an equivalent Stanton number can be defined as:

$$N_{st} = \frac{\rho h'}{G} = \frac{N_{Sh}}{N_{Re} N_{Sc}} = \frac{\text{mass actually transferred}}{\text{total mass flux}}$$

where

$$N_{Nu} = \frac{hDe}{k} = \frac{\text{total heat transfer}}{\text{conduction heat transfer}} = \text{Nusselt number}$$

$$N_{Re} = \frac{DeG}{u} = \frac{\text{inertial force}}{\text{viscous force}} = \text{Reynold number}$$

$$N_{Pr} = \frac{C_p u}{k} = \frac{\text{momentum diffusivity}}{\text{thermal diffusivity}} = \text{Prandtl number}$$

$$N_{Sh} = \frac{h'De}{D} = \frac{\text{mass diffusivity}}{\text{molecular diffusivity}} = \text{Sherwood number}$$

$$N_{Sc} = \frac{u}{\rho De} = \frac{\text{momentum diffusivity}}{\text{molecular diffusivity}} = \text{Schmidt number}$$

The use of the mass transfer coefficient h' is analogous to the heat transfer coefficient h as shown below.

$Q = h \Delta T$ heat transfer

$G^t = h' \Delta C$ mass transfer

where

Q	= heat flux	BTU/hr ft^2
h	= heat transfer coefficient	BTU/hr ft^2 ^oF
T	= temperature	^oF
G^t	= turbulent mass flux	lb/hr ft^2
h'	= mass transfer coefficient	ft/hr
C	= concentration	lb/ft^3

The equivalent Stanton number can readily be obtained without defining an effective subchannel separation distance. In order to predict turbulent mixing rates in rod bundle geometries, data are necessary on all types of interacting subchannels for various gap widths and rod diameters.

Single phase water turbulent mixing data obtained here are tabulated in Table 1, Appendix I. Single phase air turbulent mixing data are recorded in Table 2, Appendix I.

Since there was a difficulty in defining a proper distance term in the first correlation method, the equivalent Stanton number approach is employed here. All the single phase mixing data are plotted

as a function of log N_{st} versus log N_{Re} in Fig. 6.1. An appreciable entrance effect is apparent. In Fig. 6.2 the single phase air data were crossplotted as N_{st} versus the number of equivalent diameters of interconnection length, (L/D). The air turbulent mixing data and water turbulent mixing data overlap to form a continuous curve. This was expected since the Schmidt numbers for air and water are approximately equal. An exponential decrease in N_{st} was found for increasing L/D in Fig. 6.2. This effect is believed to be due to two factors. The first is the high initial mass transfer rate as the concentration profile is being developed. This is analogous to entrance effects in heat transfer, for example when the heat transfer coefficient is very high in the case of a cold fluid entering a channel with a high uniform temperature. The second factor is the increased turbulence when the two fluid streams meet at the upstream edge of the interconnection length.

In order to remove entrance effects in this analysis the average mixing rate for the last ten inches of the fourteen inch interconnection length was determined as follows. Mixing rate values for the four inch length were subtracted from those of the fourteen inch length. Then this value was used to calculate an average N_{st} over a length starting 4 inches downstream of the upstream edge of the interconnection length. The results are shown in Fig. 6.3 where N_{st} is found to vary as $N_{Re}^{-.13}$. This value is in agreement with the expected range for the exponent according to the mass-momentum transfer analogy [1]. This analogy predicts that the N_{st} should be proportional to the square root of friction factor. For turbulent flow $\sqrt{f} \propto (N_{Re})^{-.1}$.

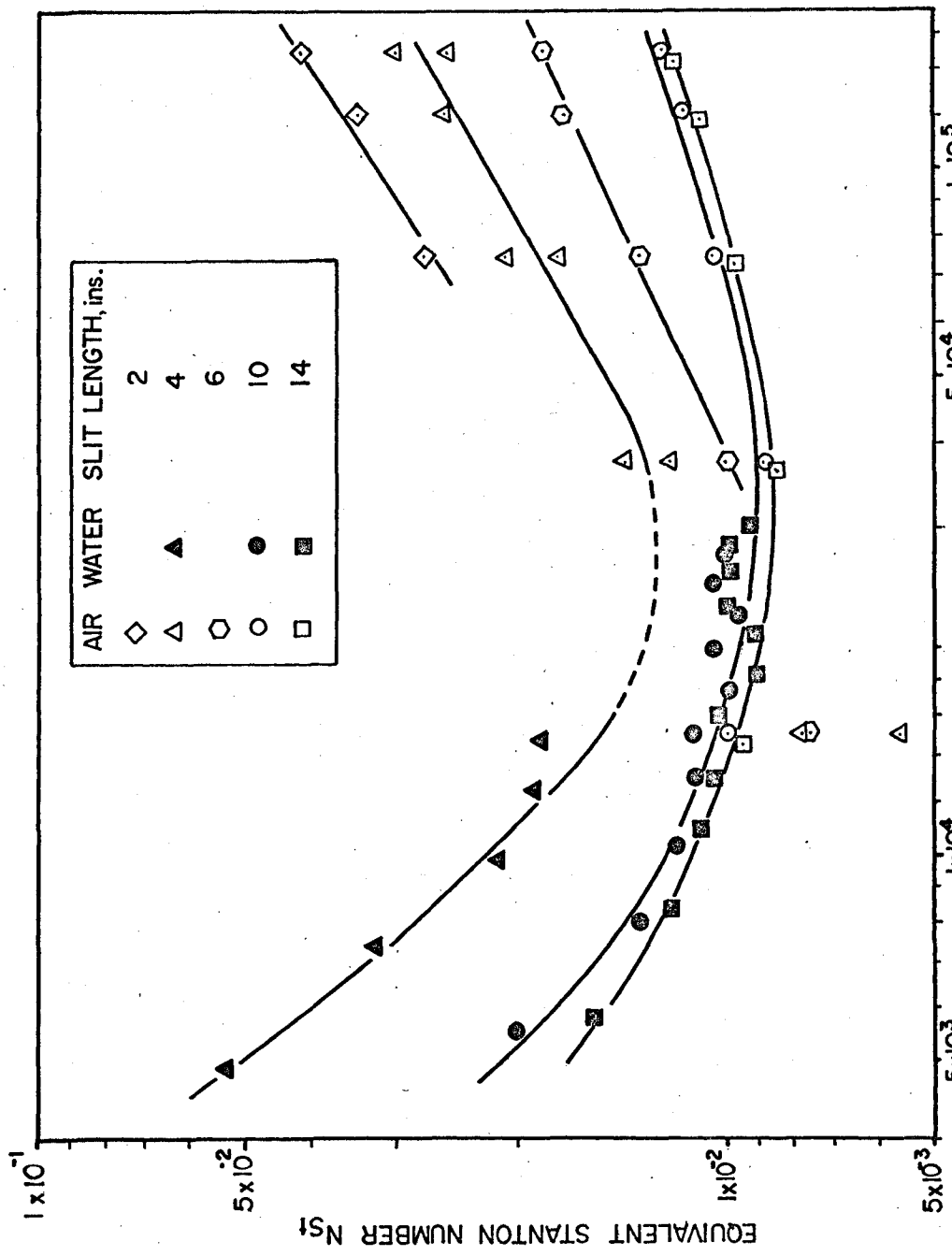

FIG: 6.1

Single Phase Mixing Data N_{St} versus N_{Re}

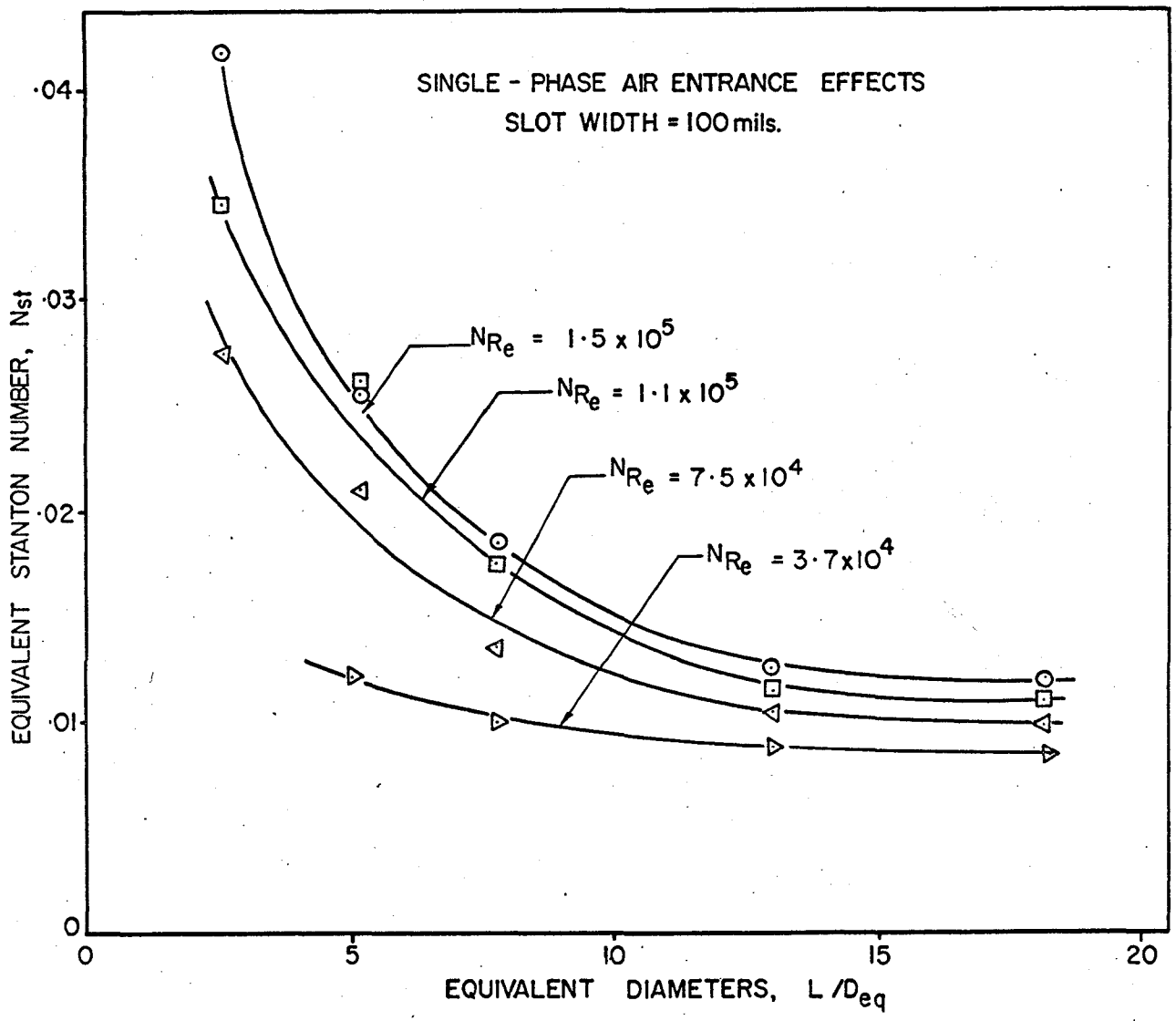

FIG. 6.2 Single Phase Air Entrance Effects

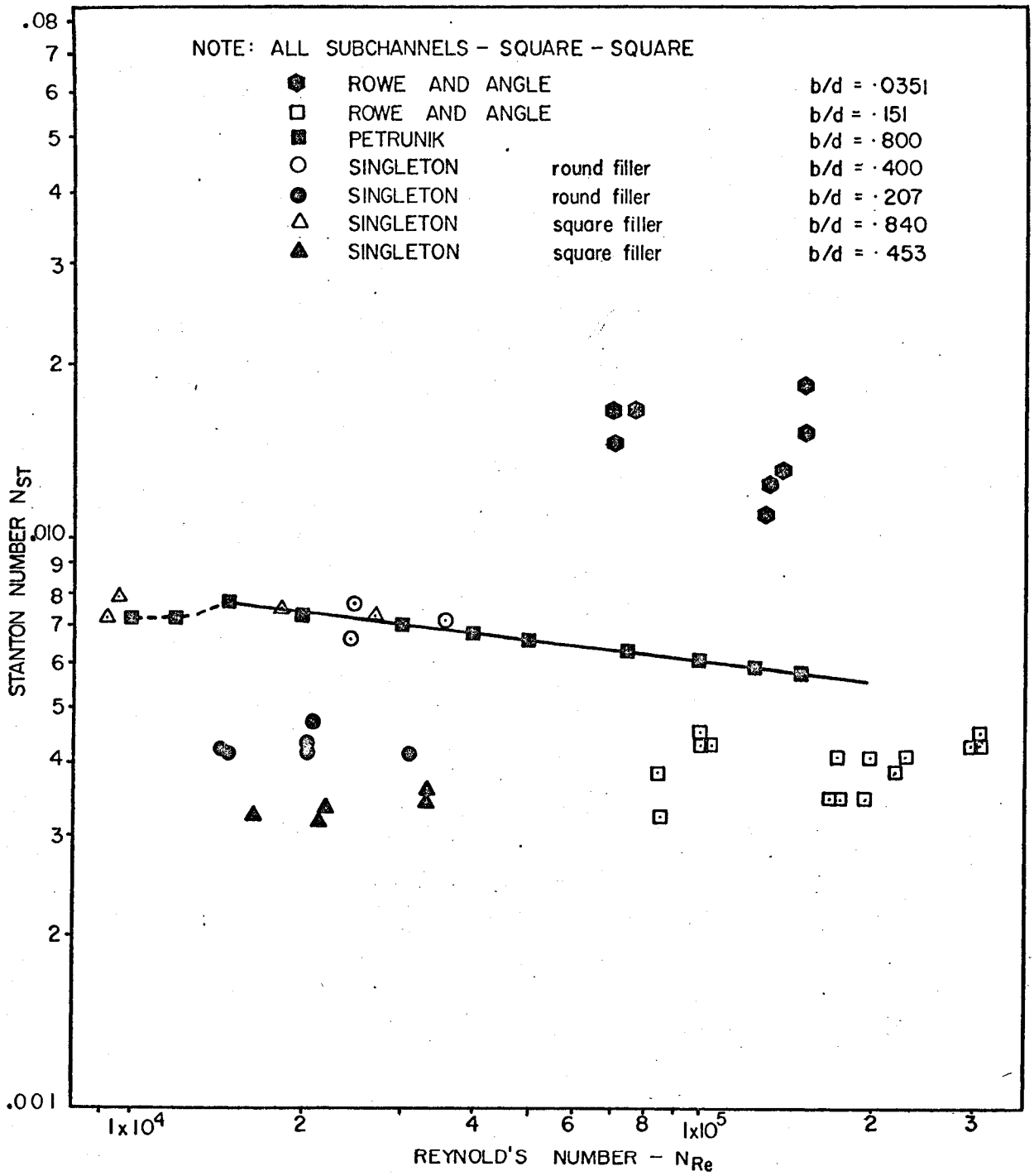

FIG. 6.3

Comparison of Single Phase Data N_{St} versus N_{Re}

The data for the ten inch interconnection length were slightly low. It was found that the O-ring seal around the dividing strip was too tight at the centre of the interconnection length which could have caused bowing. Hence a modified Stanton number was not calculated for the ten inch interconnection length.

For the four inch interconnection length, the air mixing rates were determined for gaps of 40 and 100 mils. The mixing rates were found to be proportional to the gap width. The data are plotted in Fig. 6.4. These results however do not conclusively indicate that mixing rate is directly proportional to the gap width as they may have been influenced by entrance effects.

All data considered here are for square-square subchannel arrays. The available data are plotted in Fig. 6.3. Singletons data has been reanalyzed (See Appendix III) for purpose of comparison. Also the available square-square array subchannel data have been compared with the correlation predictions of St. Pierre [11], Bowring [13], Rogers [12] and Rowe and Angle [24] in Fig. 6.5. The results are tabulated in Appendix II. Rogers noted that his original correlation [25], based on multi-rod bundle experiments, predicted significantly higher mixing rates than the correlation based on subchannel data. However these higher mixing rates in rod bundle geometries could be due to spacers and end plates which are absent in the two channel experiments. The results of Rogers modified correlation were plotted in Fig. 6.5. This is a tentative correlation as Rogers presently is reanalyzing available mixing data. Values of Rogers original correlation [12] and

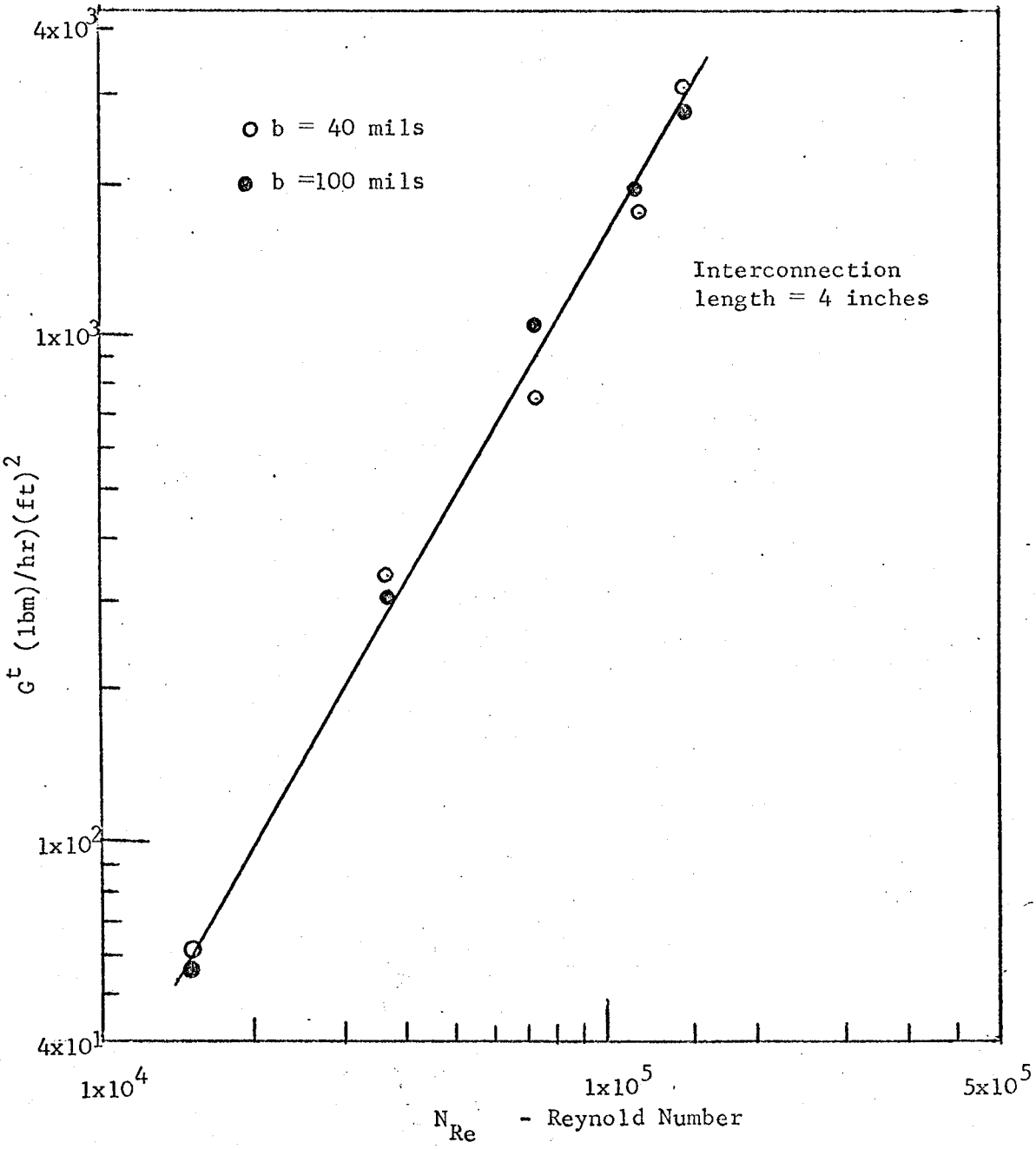

FIG. 6.4

Effect of Gap Width on 4 inch Interconnection Length

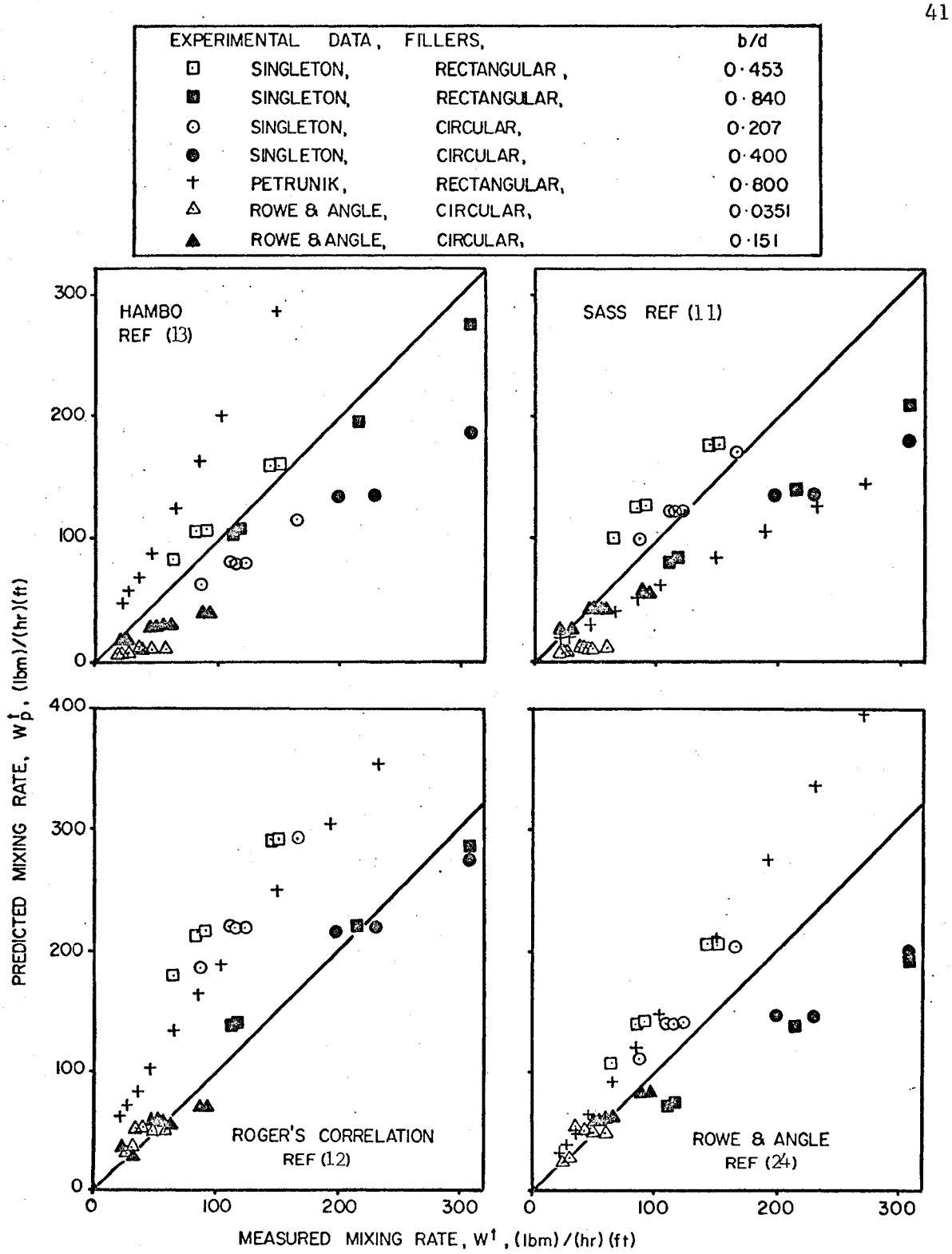

TWO CHANNEL TURBULENT MIXING DATA FOR SQUARE - SQUARE ARRAYS

FIG. 6.5

Comparison of Mixing Data with Correlation

Moyers correlation [26] are given in Appendix II but are not plotted as the former were too high and the latter too low.

It is apparent from Fig. 6.5 that no one correlation adequately predicts mixing rates for all geometries. More data are required to account for the effects of gap width, gap shape, rod diameter, subchannel array and centroidal distance.

All the single-phase data averaged for the last ten inches of the fourteen inch interconnection length can be correlated as $N_{st} = .027\ N_{Re}^{-.13}$ over the N_{Re} range 1×10^4 - 1.5×10^5.

B. Two Phase Data

Two-phase air-water turbulent mixing was studied using an interconnection length ten inches long and 100 mils wide. Because of the entrance effects in this study the results are best considered relative to the single phase mixing rates with the same interconnection length and gap. The data are tabulated in Table 3, Appendix I.

Mixing rates were determined simultaneously for both the air and the water using separate tracers. The gas mixing rate ω^t_{gt} remained approximately constant when the mass flux was fixed and the quality varied from 20 to 100% (See Fig. 6.6). The air mixing rates under two phase flow conditions were less than those for single phase flow at the same total mass flux.

Significantly higher water mixing rates, $\omega^t_{\ell t}$, were measured at the lower qualities. As the quality was increased for a fixed mass flux, the mixing rate dropped exponentially as shown in Fig. 6.6. Since laminar flow conditions would have existed for the single phase water

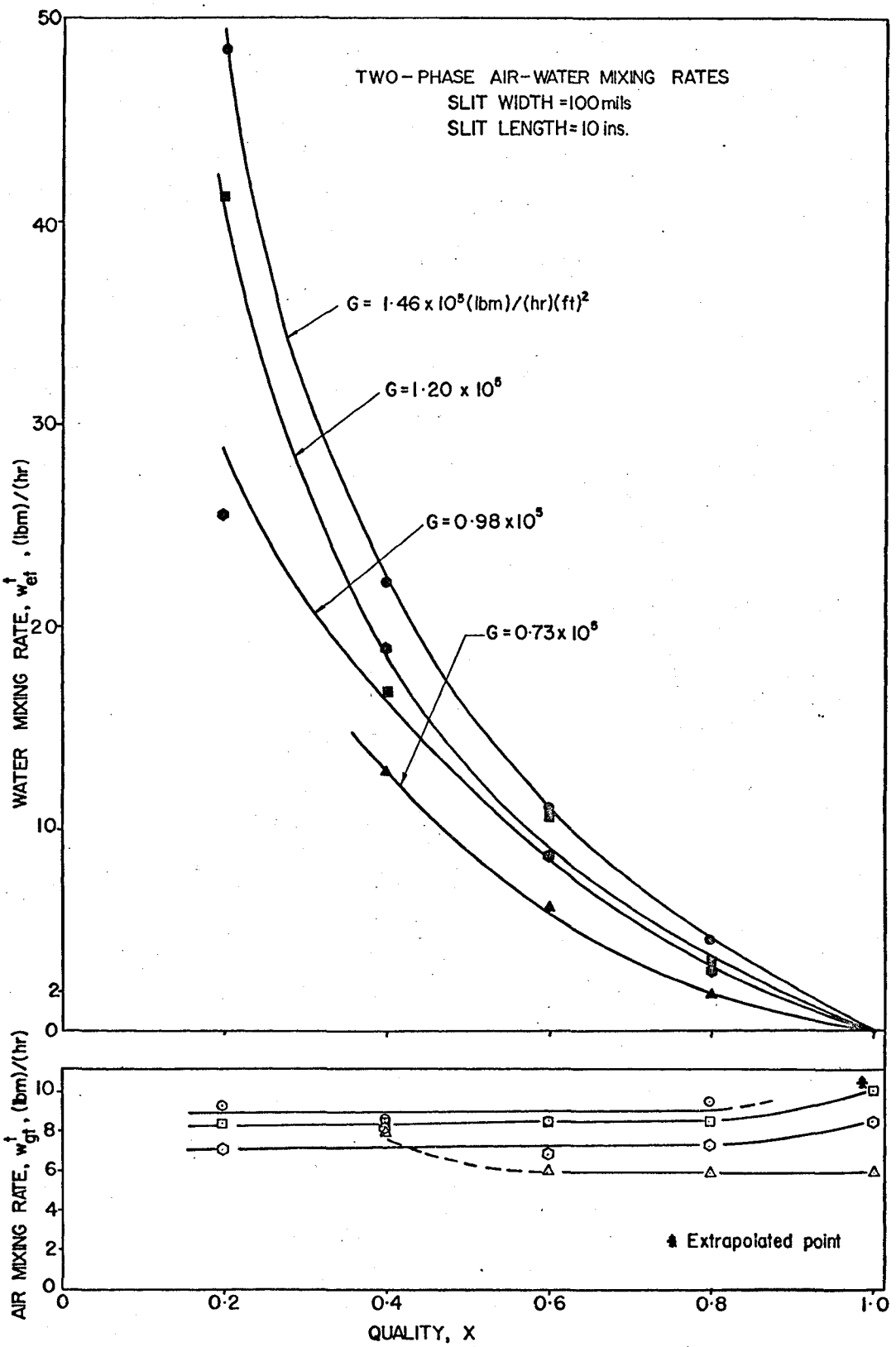

FIG. 6.6

Two-Phase Air-Water Mixing Rates

mixing rates at the same mass flux as the two-phase runs, they were not compared. However, the water mixing rates relative to the total water flow for a quality of 20% were appreciably higher than any single phase water mixing rates.

In Fig. 6.7 are shown the percentages of the air and water in the subchannel which mixed. At a fixed mass flux of 1.2×10^6 $(lbm)/(hr)(ft)^2$, the percentage of water which mixed decreased rapidly from approximately 10% at a quality of 20% to 4% at 80% quality. However, the percentage of air which mixed initially decreased from 8% at 20% quality to 2% at x=80% - then increased to 3% for single phase air flow or 100% quality. This behaviour was observed at all the mass fluxes studied. The increase in percentage air mixing from 80% quality to 100% quality is most likely due to the absence of the water film on the interconnection length, which effectively decreased the area for air mixing.

It is postulated that these high values of mixing rates at the low qualities are the result of the transition from slug to annular flow. As was indicated in Fig. 3.3 the data points at a quality of 20% are just above the transitional curve on the flow regime map. The lowest mass flux at a quality of 20% was not taken as the flow was visually observed to be unstable. The air velocity was not sufficient to maintain annular flow and the wavy film on the wall periodically broke down to bridge the core. Some liquid downflow was also observed.

Investigations have been made of the air-water interface in a horizontal rectangular duct by Bemberis [31]. He allowed air to flow over a liquid surface under co-current flow conditions. As the air

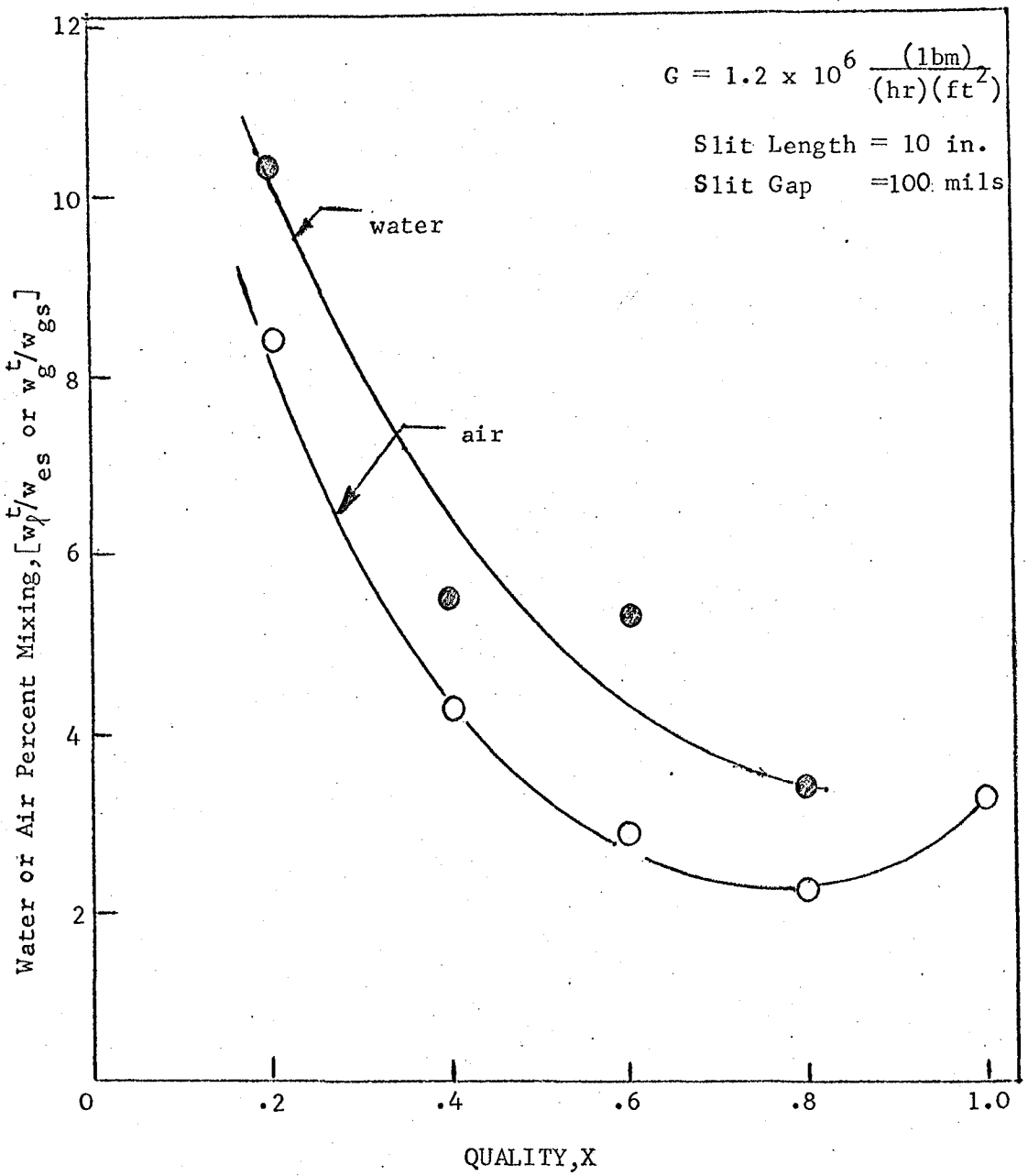

FIG. 6.7

Air and Water Percentage Mixing Rates

velocity over the liquid surface increased for fixed water flowrates, the following observations were made of the liquid-gas interface:

(i) smooth flow

(ii) ripples appeared

(iii) the liquid surface was criss-crossed by ripple like waves oblique to the duct wall.

(iv) large waves (roll waves) travelled over the liquid surface at a rate several times that of the average liquid velocity.

(v) liquid was entrained into the air.

The most important observation of Bemberis is that of the formation of roll waves which have been observed often in two-phase flow. As the gas velocity increased, the roll waves grew smaller but more frequent. Entrainment takes place when the gas strips off the top of the waves. The size of the droplets entrained increased with increasing gas velocity.

In this investigation at a quality of 20% waves were observed along the channel walls much like the roll waves described by Bemberis. The effect of interaction between large amplitude roll waves from each subchannel could explain the high water mixing rates. These waves would also affect mixing in rod bundles. The data of Rowe and Angle for two phase mixing [24] between square-square subchannels show a peak in mixing at low qualities. The flow regime maps of Bergles and Suo [32] were used to determine the transition from slug to annular flow. The peak in mixing occurred at the transition. Also, in Rowe and Angles' boiling mixing experiments for a triangular-square array, there was no increase in mixing for two phase runs compared to single phase runs for a gap width of 20 mils.

It is possible that the effect of the roll waves (which have peak heights measured to be as high as 80 mils [33]) could have been minimized by the small gap width since the interconnection length at the gap was filled with liquid. In the larger gap width of 84 mils, mixing increased due to the interaction of the roll waves from each channel.

C. Two-Phase Pressure Drop Data

The two-phase pressure drop data were compared with the Lockhart-Martinelli correlation [34]. This correlation is based on an empirical analysis of pressure drop data and is subdivided into four sections, according to the Reynold's number of each phase flowing alone in the channel. The correlation gives the transition to turbulent flow at $N_{Re} = 2000$ and the transition to laminar flow at $N_{Re} = 1000$. The region $1000 < N_{Re} < 2000$ is defined as the transition region. In the pressure drop calculations it was found that the correlation was much better if the transition was defined at $N_{Re} = 1000$.

The comparison of the experimental data with the correlation is given in Appendix IV. The greatest deviation is at a quality of 80%. This is expected as the correlation was developed for annular flow.

VII. CONCLUSIONS

Experimental measurements have been made of turbulent mixing rates for single phase air, single phase water, and two-phase air-water mixtures. The turbulent mixing data exhibited entrance effects similar to those previously observed in heat transfer under analogous conditions. The single phase mixing data were correlated as $N_{st} = 0.027\ N_{Re}^{-.13}$. The slope of -.13 in the correlation closely agreed with that which would be predicted employing the mass-momentum analogy. The experimental mixing rate data when compared with existing correlations, were all found to be inadequate for predicting mixing rates for the various subchannel arrays.

Two-phase mixing rates (expressed as a percentage of subchannel flow) increased with decreasing quality and decreasing mass flux. It is postulated that the increased mixing is related to the slug-annular transition and the effect of high amplitude roll waves. The percentage of water mixing was always greater than that for air.

Additional turbulent mixing data are required for both single and two-phase flow conditions in order to determine mixing rates for all types of subchannel arrays.

NOMENCLATURE

Dimensions are given in terms of mass(M), length(L), time(t) and temperature(T).

A	channel area	L
b	gap width	L
C	concentration of tracer	M/L^3
C_p	heat capacity	$\frac{L}{t^2T}$
d	rod diameter	L
De	equivalent diameter	L
D	molecular diffusivity	L^2/t
E_H	turbulent diffusivity for heat	L^2/t
E_M	turbulent diffusivity for mass	L^2/t
G^t	turbulent mixing flux	M/L^2t
G	channel mass flux	M/L^2t
h	heat transfer coefficient	M/t^3LT
h'	mass transfer coefficient	L/t
J_A	mass flux of A	M/L^2t
k	thermal conductivity	M/t^3T
L	channel length	L
N_{Nu}	Nusselt number	
N_{Pe}	Peclet number	
N_{Pr}	Prandtl number	
N_{Re}	Reynolds number	
N_{Sc}	Schmidt number	

N_{Sh}	Sherwood number	
N_{St}	Stanton number	
Q	heat flux	M/t^3L
R_{eq}	equivalent radius	L
r	radial distance	L
<V>	average velocity	L/t
ω_{ℓ}^{t}	liquid turbulent mixing rate	M/t
ω_{g}^{t}	gas turbulent mixing rate	M/t
$\omega_{\ell t}^{t}$	liquid two-phase turbulent mixing rate	M/t
ω_{gt}^{t}	gas two-phase turbulent mixing rate	M/t
X	quality	
z	intersubchannel distance	L

Greek Symbols

ρ	density	M/L^3
β	Stanton Number (Rowe and Angle)	
ψ	$1/N_{Pe}$	

Subscripts

g	gas
gt	gas in two-phase flow conditions
ℓ	liquid
ℓt	liquid in two-phase flow conditions

REFERENCES

[1] Rogers, T.J. and Todreas, N.E., Coolant Interchannel Mixing in Reactor Fuel Rod Bundles, Single Phase Coolants, to be presented ASME Winter Meeting (1968).

[2] Sherwood, T.K., Heat Transfer, Mass Transfer, and Fluid Function, I.E.C. 43, No. 10, pp 2077-2084 (1950).

[3] Diessler, R.G., Analysis of Turbulent Heat Transfer, Mass Transfer, and Friction in Smooth Tubes at High Prandtl and Schmidt Numbers, NACA - 1210, (1954).

[4] Wilson, H.A., Proc. Cambridge. Phil. Soc., 12, 406, (1904).

[5] Towle, W.L., and Sherwood, T.K., Eddy Diffusion, Mass Transfer in the Central Portion of a Turbulent Air Stream, I.E.C. 31, No. 4, pp 457, 462 (1939).

[6] Slember, R.J., M.Sc. Thesis, Mechanical Engineering, University of Pittsburg, (1958), also WAPD T-653 (1958).

[7] McCarter, R.J., Stutzman, L.F., and Koch, H.A. Jr., Temperature Gradients and Eddy Diffusivities in Turbulent Fluid Flow, I.E.C. 41, No. 6, pp 1290 - 1295 (1949).

[8] Pfennigwerth, P.L., and Steer, R.W., Preliminary Air-Water Mixing Tests, WAPD-TM-492 (1965).

[9] Sherwood, T.K., and Woertz, B.B., Mass Transfer Between Phases, I.E.C. 31, No. 8, pp 1034 - 1041 (1939).

[10] Dhanck, A.M., Momentum and Mass Transfer by Eddy Diffusion in a Wetted-Wall Channel, A.I.Ch.E.J. 4, No. 2, pp 190 - 196 (1958).

[11] St. Pierre, C.C., Sass Code I, Subchannel Analysis for the Steady-State, APPE-41, (1966).

[12] Rogers, T.J., and Tarasuk W.R., A Generalized Correlation for Natural Turbulent Mixing of Coolant in Fuel Bundles, Presented A.N.S. meeting, Toronto, Ontario, (1968).

[13] Bowring, R.W., Hambo, A., Computer Program for the Subchannel Analysis of the Hydraulic and Burnout Characteristics of Rod Clusters. Atomic Energy Establishment, Winfrath, Dorset (1968) AEEW-R-582.

[14] Rowe, D.S., Cross-Flow Mixing Between Parallel Flow Channels During Boiling, Part I, COBRA Computer Program for Coolant Boiling in Rod Arrays, BNWL-371, Pt. 1, Pacific Northwest Laboratory, Richland, Washington, 1967.

[15] Clarke, G.J., Mixing Studies of Types C19A14B, C19A14C, and C19x80 Fuel Bundles, AECL Report TDVI-19, (1961).

[16] Rogers, J.T., and Tarasuk, W.R., Inter-sub-channel Coolant Mixing in Close-packed Reactor Fuel Bundles Part I - Natural Mixing, CGE Report R64CAP29-I. (1966).

[17] Collins, R.D., and France, J., Mixing of Coolant in Channels between close packed Fuel Elements, IGR-TN/CA-847, (1958).

[18] Bishop, A.A., Nelson, P.A., and McCabe Jr., E.A., Thermal and Hydraulic Design of the CUTR Fuel Assemblies, Westinghouse Report CUNA-115, p 48 (1962).

[19] Nelson, P.A., Bishop, A.A., and Tong L.S., Mixing in Flow Parallel to Rod Bundles Having a Square Lattice, Westinghouse Report, WCAP-16 (1960).

[20] Dean, R.A., Coolant Mixing in Open Lattice Reactor Core, Westinghouse Report, WCAP-3735 (1963).

[21] Biggs, W.M., and Rust, J.H., A Study of Interchannel Mixing Employing Activation Analysis, Trans. ANS 10, No. 2, p 655 (1967).

[22] Singleton, N.R., M.Sc. Thesis, Mechanical Engineering, University of Pittsburgh (1963).

[23] Rowe, D.S. and Angle C.W., Crossflow Mixing Between Parallel Flow Channels During Boiling Part II, Measurement of Flow Enthalpy in Two Parallel Channels, BNWL-371- Part 2, Pacific Northwest Laboratory, Richland, Washington (1967).

[24] McPherson D., Personnal Communication August (1968).

[25] Rogers, T.J., Personal Communication (August 1968).

[26] Moyer, C.B., Coolant Mixing in Multirod Fuel Bundles, Riso Report No. 125, (1964) (issued 1966).

[27] McPherson, D., Personal Communication (July 1968).

[28] Wallis G., Eleventh Advanced Seminar, Two-Phase Gas Liquid Flows, A.I.Ch.E., New York, pp 1-33(1967).

[29] Moeck, E.O. Personal Communication (June 1967).

[30] ASME Power Test Code Supplement, PTC 19.5; 4, (1959).

[31] Bemberis, I., Quartly Progress Report, NYO-3114-5 October-December (1964).

[32] Bergles A.E., and Suo, M., Investigation of Boiling Water Flow Regimes at High Pressures, NYO-3304-8, (1966).

[33] Dukler A.E., Two-Phase Gas Liquid Flows, Eleventh Advanced Seminar AIChE., New York (1967).

[34] Lockhart, R.W., and Martenelli R.C., Proposed Correlation of Data for Isothermal Two-Phase Two Component Flow in Pipes, Chem. Eng. Progr, 45, pp 39-48 (1947).

[35] Perry, J.H., Chemical Engineer's Handbook , McGraw-Hill Pub., pp 14-16 (1963).

APPENDIX I

SINGLE PHASE MIXING DATA

APPENDIX I

Single Phase Mixing Data

The run numbers recorded in the following tables were coded as below. For example in Run 22RO we have:

Interconnection Length	Interconnection Width	Subchannel Injection	Quality
2	2	R	O

Number Code	Interconnection length (inches)
1	2
2	4
3	6
4	10
5	14

Number Code	Interconnection width (mils)
1	40
2	100

Letter Code	Subchannel Injection
L	left
R	right

Number Code	= Quality %
0	0
1	100
2	20
4	40
6	60
8	80

Methane concentrations are given in moles of methane per mole of mixture. Potassium concentrations are given as lb of potassium per lb of water.

TABLE II

SINGLE PHASE WATER MIXING DATA

RUN NUMBER	MASS FLOW lb/hr	MASS FLUX lb/hr.ft^2	REYNOLDS NUMBER	STANTON NUMBER	MIXING RATE lb/hr	TEMPERATURE °F	TRACER CONCENTRATION LEFT	TRACER CONCENTRATION RIGHT
22R0	1640	200489	4855	.06170	34.36	58	.000088	.002100
22L0	1640	200489	4855	.04511	25.12	58	.002350	.000072
22R0	2460	300733	7424	.03313	27.67	60	.000045	.002000
22L0	2460	300733	7424	.03213	26.84	60	.002200	.000048
22R0	3280	400978	9899	.01929	21.49	60	.000019	.001450
22L0	3280	400978	9899	.02492	27.75	60	.001300	.000022
22R0	3280	400978	9899	.02002	22.30	60	.000017	.001250
22L0	3280	400978	9899	.02209	24.60	60	.001400	.000021
22R0	4100	501222	12138	.01963	27.33	58	.000020	.001500
22L0	4100	501222	12138	.01897	26.41	58	.001475	.000019
22R0	4100	501222	12374	.02142	29.82	60	.000024	.001650
22L0	4100	501222	12374	.01646	22.91	60	.001700	.000019
22R0	4100	501222	12254	.01902	26.48	59	.000015	.001200
22L0	4100	501222	12254	.01929	26.86	59	.001450	.000019
22L0	4920	601467	14565	.01633	27.29	58	.001262	.000014
22R0	4920	601467	14565	.02098	35.06	58	.000018	.001263
42L0	1640	200489	5542	.01656	23.05	71	.003175	.000089
42R0	1640	200489	5542	.02272	31.64	71	.000129	.003350
42L0	1640	200489	5424	.01738	24.20	69	.003050	.000090
42R0	1640	200489	5424	.02290	31.89	69	.000105	.002700
42R0	2460	300733	8050	.01372	28.65	68	.000044	.001900
42L0	2460	300733	8050	.01303	27.21	68	.002000	.000044
42L0	3280	400978	10405	.01164	32.41	65	.001050	.000021
42R0	3280	400978	10405	.01191	33.16	65	.000023	.001125
42R0	4100	501222	13006	.01158	40.32	65	.000015	.000750
42L0	4100	501222	13006	.01080	37.58	65	.000750	.000014
42R0	4920	601467	15143	.01213	50.68	62	.000026	.001250
42L0	4920	601467	15143	.01046	43.70	62	.001140	.000020
42L0	5740	701711	17493	.00969	47.22	61	.001170	.000019
42R0	5740	701711	17493	.01039	50.61	61	.000020	.001120
42R0	6560	801956	19992	.01111	61.90	61	.000029	.001550
42L0	6560	801956	19992	.01017	56.66	61	.001780	.000031
42R0	7380	902200	22491	.01032	64.68	61	.000030	.001740
42L0	7380	902200	22491	.00885	55.47	61	.001530	.000023
42L0	8200	1002445	24990	.01079	75.11	61	.001160	.000021
42R0	8200	1002445	24990	.01046	72.79	61	.000024	.001380
42R0	9020	1102689	27489	.01038	79.48	61	.000022	.001220
42L0	9020	1102689	27489	.00990	75.81	61	.001160	.000019
52R0	1640	200489	5794	.01658	32.32	75	.000113	.002875
52L0	1640	200489	5794	.01472	28.68	75	.003925	.000137
52L0	2460	300733	8405	.01274	37.24	72	.002075	.000063
52R0	2460	300733	8405	.01254	36.67	72	.000063	.002125
52R0	3280	400978	10965	.01081	42.16	70	.000039	.001525
52L0	3280	400978	10965	.01133	44.17	70	.001475	.000040
52L0	4100	501222	13417	.01038	50.56	68	.001100	.000027
52R0	4100	501222	13417	.01096	53.41	68	.000030	.001138
52R0	4920	601467	16101	.01052	61.50	68	.000023	.000938
52L0	4920	601467	16101	.01027	60.07	68	.001025	.000025
52L0	5740	701711	18396	.00869	59.27	66	.001150	.000024
52R0	5740	701711	18396	.01038	70.82	66	.000029	.001163
52R0	6560	801956	20809	.00933	72.71	65	.000027	.001200
52L0	6560	801956	20809	.00979	76.29	65	.000963	.000022
52R0	7380	902200	23410	.01009	88.48	65	.000022	.000900
52L0	7380	902200	23410	.01010	88.56	65	.000750	.000018
52L0	8200	1002445	26280	.01014	98.83	66	.000838	.000020
52R0	8200	1002445	26280	.00975	95.02	66	.000020	.000860
52R0	9020	1102689	28323	.01001	107.31	64	.000019	.000786
52L0	9020	1102689	28323	.01008	108.05	64	.000763	.000018
52L0	9840	1202934	30898	.00964	112.70	64	.000750	.000017
52R0	9840	1202934	30898	.00904	105.75	64	.000019	.000863

TABLE I2

SINGLE PHASE AIR MIXING DATA

RUN NUMBER	MASS FLOW lb/hr	MASS FLUX lb/hr.ft^2	REYNOLDS NUMBER	STANTON NUMBER	MIXING RATE lb/hr	TEMPERATURE °F	TRACER CONCENTRATION LEFT	RIGHT
12L1	208	50813	74132	.02821	1.99	70	.027500	.000263
12R1	209	50989	74389	.03011	2.13	70	.000343	.033400
12L1	209	50955	74339	.02242	1.59	70	.032500	.000247
12R1	209	50905	74266	.02883	2.04	70	.000300	.030700
12L1	312	76245	111235	.02824	2.99	70	.028100	.000269
12R1	312	76123	111058	.03758	3.97	70	.000121	.025200
12L1	313	76316	111339	.03234	3.43	70	.029700	.000326
12R1	312	76245	111235	.03930	4.16	70	.000173	.028000
12L1	414	100989	147334	.04000	5.61	70	.010300	.000221
12R1	413	100918	147231	.05192	7.28	70	.000264	.015000
12R1	415	101354	147867	.03665	5.16	70	.000282	.022700
12L1	414	101131	147542	.03829	5.38	70	.018400	.000244
21R1	42	10358	15226	.00546	.06	65	.000031	.061300
21L1	42	10358	15225	.01551	.18	65	.001100	.000257
21L1	42	10357	15224	.00454	.05	65	.001100	.000075
21L1	43	10390	15273	.00155	.02	65	.006800	.000028
21L1	43	10410	15302	.00326	.04	65	.000100	.000062
21R1	43	10391	15275	.00667	.08	65	.000121	.066900
21R1	43	10404	15293	.03311	.38	65	.000615	.068500
21R1	42	10297	15137	.00600	.07	65	.000043	.051000
21L1	42	10320	15170	.01359	.16	65	.054400	.000202
21L1	42	10289	15124	.00327	.04	65	.049600	.000044
21L1	105	25558	37569	.01226	.35	65	.038200	.000127
21R1	105	25566	37582	.01140	.32	65	.000120	.038800
21L1	105	25517	37509	.01786	.51	65	.035300	.000171
21L1	105	25616	37655	.01494	.43	65	.042200	.000171
21R1	105	25617	37657	.01264	.36	65	.000145	.042300
21R1	105	25739	37835	.01501	.43	65	.000200	.050600
21L1	105	25588	37613	.00997	.28	65	.040300	.000109
21R1	209	51111	75133	.01805	1.03	65	.000186	.038000
21L1	209	51101	75118	.01408	.80	65	.037700	.000144
21L1	209	50944	74887	.00925	.52	65	.032300	.000081
21L1	209	50942	74884	.01248	.71	65	.032200	.000109
21R1	209	50929	74865	.01815	1.03	65	.000150	.031700
21R1	209	50967	74920	.01721	.97	65	.000154	.033000
21R1	313	76362	112251	.02446	2.08	65	.000205	.030900
21R1	313	76360	112247	.01766	1.50	65	.000148	.030900
21L1	313	76323	112193	.02335	1.98	65	.030000	.000190
21L1	313	76278	112127	.01755	1.49	65	.029000	.000138
21R1	313	76363	112251	.02613	2.22	65	.000219	.030900
21R1	313	76362	112251	.02530	2.15	65	.000212	.030900
21R1	311	75941	111632	.02377	2.01	65	.000136	.021100
21L1	311	75950	111644	.02389	2.02	65	.021300	.000138
21L1	415	101383	149030	.03086	3.48	65	.023300	.000195
21R1	415	101405	149064	.03018	3.40	65	.000194	.023700
21R1	416	101457	149139	.02953	3.33	65	.000197	.024600
22L1	43	10405	15157	.00622	.18	71	.069000	.000291
22R1	43	10393	15139	.00415	.12	71	.000189	.067100
22L1	42	10319	15168	.00723	.21	65	.054500	.000267
22R1	42	10318	15168	.00506	.15	65	.000187	.054500
22R1	105	25572	37251	.00845	.80	71	.000224	.039100
22L1	105	25582	37266	.01624	1.15	71	.039400	.000436
22R1	105	25550	37558	.01227	.87	65	.000312	.037500
22L1	105	25567	37494	.01171	.83	65	.034500	.000274
22L1	208	50614	74022	.01620	2.29	71	.027500	.000302
22R1	208	50807	74011	.02471	3.49	71	.000454	.027100
22R1	208	50770	74631	.01481	2.09	65	.000261	.026000
22L1	208	50734	74578	.02350	3.31	65	.024600	.000392
22L1	207	50591	74368	.01902	2.67	65	.019700	.000254
22R1	207	50583	74356	.02744	3.86	65	.000359	.019300
22R1	311	75986	110692	.02045	4.32	71	.000385	.022000
22L1	311	75980	110683	.03134	6.61	71	.021700	.000461
22R1	311	75783	111400	.02607	5.49	65	.000304	.017200
22L1	311	75851	111500	.02448	5.16	65	.018400	.000312
22R1	310	75729	111320	.03024	6.36	65	.000328	.015900
22L1	310	75765	111372	.02327	4.90	65	.016400	.000265
22L1	413	100881	148292	.01997	5.60	65	.014400	.000195
22R1	413	100855	148255	.02621	7.34	65	.000247	.013900
22L1	413	100838	148229	.02484	6.96	65	.013400	.000229
22R1	413	100841	148234	.03102	8.69	65	.000286	.013600

RUN NUMBER	MASS FLOW lb/hr	MASS FLUX lb/hr.ft^2	REYNOLDS NUMBER	STANTON NUMBER	MIXING RATE lb/hr	TEMPERATURE °F	TRACER CONCENTRATION LEFT	TRACER CONCENTRATION RIGHT
32R1	43	10468	15295	.00587	.26	69	.000473	.0793
32L1	43	10418	15222	.00922	.40	69	.000600	.0006
32L1	42	10358	15111	.00925	.40	70	.000600	.0005
32R1	42	10341	15087	.00608	.26	70	.000360	.0582
32L1	106	25794	37687	.00985	1.06	69	.000600	.0005
32R1	105	25727	37590	.00938	1.01	69	.000472	.0495
32R1	106	25823	37674	.00987	1.06	70	.000562	.0560
32L1	106	25882	37759	.00847	.91	70	.000600	.0005
32R1	209	51019	74544	.01052	2.24	69	.000370	.0346
32L1	209	51012	74535	.01584	3.37	69	.000200	.0005
32L1	210	51257	74780	.01200	2.56	70	.000700	.0005
32R1	210	51268	74795	.01584	3.38	70	.000491	.0429
32R1	312	76139	111248	.01512	4.80	69	.000392	.0255
32L1	313	76341	111543	.01686	5.36	69	.000100	.0005
32R1	314	76586	112070	.01956	6.24	68	.000708	.0358
32L1	314	76603	112094	.02180	6.96	68	.000900	.0007
32R1	312	76219	111197	.01671	5.31	70	.000464	.0273
32L1	312	76230	111213	.01496	4.75	70	.000600	.0004
32L1	415	101201	147867	.01942	6.19	69	.000900	.0003
32R1	415	101359	148098	.01659	7.01	69	.000383	.0227
32L1	416	101493	148517	.02101	8.88	68	.000900	.0005
32R1	416	101410	148396	.02021	8.54	68	.000483	.0235
32L1	416	101422	147967	.01628	6.88	70	.000800	.0003
32R1	415	101408	147946	.01829	7.73	70	.000437	.0235
42R1	42	10326	15179	.01137	.82	65	.001058	.0549
42L1	42	10317	15166	.00867	.62	65	.000700	.0007
42L1	42	10265	14975	.00909	.65	70	.000800	.0006
42R1	42	10268	14980	.01082	.77	70	.000829	.0452
42R1	105	25508	37496	.00832	1.47	65	.000485	.0344
42L1	105	25582	37605	.00735	1.31	65	.000500	.0004
42L1	104	25445	37404	.00761	1.34	65	.000100	.0003
42R1	104	25462	37428	.01207	2.13	65	.000634	.0310
42R1	104	25468	37156	.01094	1.93	70	.000584	.0315
42L1	104	25453	37133	.00785	1.39	70	.000600	.0004
42R1	105	25584	37325	.01129	2.01	70	.000754	.0394
42L1	105	25578	37316	.00768	1.36	70	.000200	.0005
42L1	208	50645	74447	.01010	3.55	65	.000500	.0003
42R1	207	50640	74439	.01039	3.65	65	.000375	.0213
42L1	208	50725	74603	.00901	3.17	70	.000300	.0003
42R1	208	50650	73894	.01199	4.22	70	.000439	.0216
42L1	208	50673	73928	.00913	3.21	70	.000500	.0003
42L1	208	50762	74058	.00890	3.14	70	.000600	.0003
42R1	208	50738	74022	.01264	4.45	70	.000527	.0246
42R1	311	75798	111422	.01217	6.41	65	.000361	.0175
42L1	311	75797	111420	.01136	5.98	65	.000500	.0003
42L1	311	75942	111633	.01019	5.37	65	.000900	.0003
42R1	311	75942	111633	.01285	6.78	65	.000453	.0208
42R1	311	75837	111479	.01247	6.57	65	.000389	.0184
42L1	311	75817	111450	.01026	5.40	65	.000000	.0003
42L1	311	75853	110664	.01139	6.00	70	.000800	.0003
42R1	311	75877	110699	.01308	6.89	70	.000428	.0192
42R1	311	75928	110772	.01215	6.40	70	.000422	.0205
42L1	311	75919	110760	.00905	4.77	70	.000400	.0003
42L1	311	75935	110784	.01143	6.03	70	.000700	.0004
42R1	311	75895	110724	.01321	6.96	70	.000441	.0197
42L1	414	101128	148656	.01256	8.82	65	.000600	.0003
42R1	414	101093	148604	.01190	8.35	65	.000363	.0180
42R1	414	101125	148651	.01375	9.65	65	.000431	.0185
42L1	414	101091	148602	.01121	7.87	65	.000000	.0003
42R1	414	101090	147482	.01355	9.51	70	.000411	.0175
42L1	414	100960	147293	.01172	8.22	70	.000700	.0003
52R1	42	10142	14534	.00937	.92	82	.000525	.0236
52L1	42	10137	14526	.00965	.95	82	.000700	.0005
52L1	104	25401	36400	.00893	2.21	82	.000800	.0005
52R1	104	25417	36424	.00816	2.02	82	.000542	.0280
52R1	208	50698	72653	.00985	4.85	82	.000542	.0232
52L1	208	50719	72682	.00982	4.84	82	.000900	.0005
52L1	311	75925	108803	.01140	8.41	82	.000300	.0005
52R1	311	75962	108770	.01079	7.96	82	.000507	.0198
52R1	414	101165	144973	.01191	11.72	82	.000540	.0191
52L1	414	101165	144974	.01214	11.94	82	.000100	.0005

TABLE I3

TWO PHASE AIR-WATER MIXING DATA

RUN NUMBER	MASS FLOW lb/hr AIR	MASS FLOW lb/hr WATER	MASS FLUX lb/hr.ft^2	MIXING RATE lb/hr AIR	MIXING RATE lb/hr WATER	TEMPERATURE °F AIR	TEMPERATURE °F WATER	TRACER CONCENTRATIONS AIR LEFT	TRACER CONCENTRATIONS AIR RIGHT	TRACER CONCENTRATIONS WATER LEFT	TRACER CONCENTRATIONS WATER RIGHT
42L2	80	320	97627	7.15	25.46	67	77	.048380	.004322	.004700	.000374
42R2	80	320	97627	7.05	25.75	67	68	.004271	.048460	.000523	.006500
42L2	100	400	122034	8.69	37.92	67	78	.049380	.004292	.005000	.000474
42R2	100	400	122034	7.98	44.50	68	77	.004219	.052850	.000445	.004000
42L2	120	480	146441	8.50	47.24	68	76	.042120	.002985	.003800	.000374
42R2	120	480	146441	10.15	49.60	68	75	.003304	.039050	.000465	.004500
42L4	120	180	73220	8.19	13.87	66	68	.048560	.003313	.005400	.000416
42R4	120	180	73220	7.82	15.51	66	68	.003312	.050800	.000474	.005500
42L4	160	240	97627	8.25	17.65	64	76	.045670	.002354	.004800	.000353
42R4	160	240	97627	7.98	19.95	64	75	.002266	.045460	.000399	.004800
42L4	200	300	122034	8.52	14.38	64	73	.041070	.001750	.005800	.000278
42R4	200	300	122034	8.44	18.94	64	74	.001693	.040130	.000341	.005400
42L4	240	360	146441	8.32	18.35	70	84	.044500	.001542	.005200	.000265
42R4	240	360	146441	8.91	25.96	70	81	.001683	.045350	.000274	.003800
42L6	180	120	73220	6.26	5.78	66	66	.042000	.001460	.005340	.000257
42R6	180	120	73220	5.82	6.26	67	77	.001387	.042900	.000261	.005000
42L6	240	160	97627	6.65	6.32	62	75	.045880	.001272	.004200	.000166
42R6	240	160	97627	6.97	10.96	62	86	.001283	.044160	.000274	.004000
42L6	300	200	122034	9.48	7.66	68	75	.036280	.001147	.002800	.000107
42R6	300	200	122034	7.45	13.47	68	79	.000899	.036200	.000136	.002025
42L6	360	240	146441	9.37	8.27	67	82	.035900	.000934	.002800	.000096
42R6	360	240	146441	7.50	13.44	67	82	.000740	.035500	.000084	.001500
42L8	240	60	73220	5.94	1.68	67	64	.040570	.001004	.008000	.000224
42R8	240	60	73220	5.88	1.82	67	64	.001018	.041520	.000328	.010800
42L8	320	80	97627	8.25	2.79	67	67	.040400	.001041	.003200	.000111
42R8	320	80	97627	6.31	3.26	68	69	.000759	.038500	.000114	.002800
42L8	)	100	122034	8.66	2.62	66	66	.035560	.000770	.003400	.000089
42R8	400	100	122034	8.38	4.02	66	69	.000773	.036900	.000126	.003150
42L8	480	120	146441	9.87	3.53	71	73	.026400	.000543	.006500	.000191
42R8	480	120	146441	9.03	5.47	72	75	.000527	.028000	.000187	.004100

APPENDIX II

COMPARISON OF MIXING RATES AND EXPERIMENTAL DATA USING PROPOSED CORRELATIONS

APPENDIX II

Comparison of Mixing Rates and Experimental Data Using Proposed Correlations

The correlations given in the literature survey, Chapter II, Section E, are compared to available subchannel mixing data. The results are given in tabular form in Tables II-1 and II-2.

TABLE I

COMPARISON OF PREDICTED MIXING RATES AND EXPERIMENTAL DATA

MEASURED MIXING lb/hr.ft PETRUNIK	PREDICTED MIXING USING CORRELATIONS lb/hr.ft SASS	HAMBO	ROGERS (1)	ROGERS (2)	ROWE	MOYER	REYNOLDS NUMBER	MASS FLUX $lb/hr.ft^2$	(b/d)
22.75	17.51	46.70	72.55	63.50	34.68	9.13	10000	378125	.800
27.11	20.19	55.02	82.12	71.88	40.87	10.76	12000	453750	.800
36.54	24.05	67.26	95.58	83.66	49.96	13.15	15000	567187	.800
46.01	30.13	87.14	116.23	101.74	64.72	17.04	20000	756250	.800
65.70	41.38	125.51	153.13	134.04	93.22	24.55	30000	1134375	.800
85.33	51.84	162.61	186.22	163.00	120.77	31.80	40000	1512500	.800
103.98	61.74	198.77	216.73	189.71	147.64	38.87	50000	1890625	.800
149.36	84.80	286.31	285.54	249.93	212.65	55.99	75000	2835937	.800
194.10	106.23	370.92	347.23	303.94	275.50	72.54	100000	3781250	.800
232.39	126.51	453.42	404.13	353.74	336.77	88.67	125000	4726562	.800
271.30	145.92	534.27	457.47	400.43	396.83	104.48	150000	5671875	.800

MEASURED MIXING lb/hr.ft ROWE and ANGLE	PREDICTED MIXING USING CORRELATIONS lb/hr.ft SASS	HAMBO	ROGERS (1)	ROGERS (2)	ROWE	MOYER	REYNOLDS NUMBER	MASS FLUX $lb/hr.ft^2$	(b/d)
48.96	9.76	8.80	340.90	50.51	50.15	3.28	151300	1900000	.035
59.04	9.84	8.89	343.33	50.87	50.63	3.31	152900	1920000	.035
27.40	5.76	4.81	215.83	31.98	27.38	1.79	77230	970000	.035
28.80	6.20	5.11	234.82	34.79	29.10	1.90	69430	1020000	.035
25.24	6.26	5.16	236.63	35.06	29.37	1.92	69880	1030000	.035
28.26	6.10	5.02	231.45	34.29	28.58	1.87	68280	1000000	.035
36.36	10.33	9.17	366.38	54.29	52.22	3.42	131000	1950000	.035
41.04	10.35	9.20	366.48	54.30	52.41	3.43	133000	1960000	.035
43.20	10.22	9.12	360.25	53.38	51.94	3.40	138100	1950000	.035
57.24	41.48	27.99	166.69	56.35	60.70	16.88	219300	2060000	.151
47.88	41.30	27.05	170.38	57.59	58.65	16.31	169800	1940000	.151
56.52	40.82	26.83	167.90	56.75	58.18	16.17	174900	1930000	.151
56.16	40.63	26.70	167.15	56.50	57.89	16.09	174500	1920000	.151
47.16	40.54	26.67	166.60	56.32	57.83	16.08	176300	1920000	.151
88.20	53.72	37.64	208.86	70.60	81.62	22.69	302200	2860000	.151
88.92	54.02	37.88	209.86	70.94	82.13	22.83	304300	2880000	.151
29.63	22.84	14.09	99.31	33.57	30.55	8.49	101800	960000	.151
30.85	22.67	13.96	98.71	33.37	30.27	8.42	100400	950000	.151
22.46	24.00	14.49	106.35	35.95	31.43	8.74	84880	970000	.151
26.89	23.99	14.49	106.25	35.91	31.42	8.74	85140	970000	.151
57.24	41.38	27.96	166.09	56.14	60.64	16.86	221800	2060000	.151
61.92	42.36	28.71	169.57	57.32	62.25	17.31	227400	2120000	.151
47.52	39.90	26.55	162.32	54.87	57.56	16.00	194400	1930000	.151
57.60	40.57	27.05	164.79	55.70	58.66	16.31	197700	1970000	.151
93.96	54.03	37.95	209.58	70.84	82.30	22.88	308900	2890000	.151
29.63	22.72	14.05	98.57	33.32	30.48	8.47	104200	960000	.151

TABLE II

MEASURED MIXING lb/hr.ft	PREDICTED MIXING USING CORRELATIONS lb/hr.ft								
SINGLETON	SASS	HAMBO	ROGERS (1)	ROGERS (2)	ROWE	MOYER	REYNOLDS NUMBER	MASS FLUX $lb/hr.ft^2$	(b/d)
157.31	176.69	158.69	461.26	292.08	208.00	91.95	33400	1822625	.453
144.40	176.69	158.69	461.26	292.08	208.00	91.95	33400	1822625	.453
158.34	177.16	159.17	462.34	292.77	208.63	92.23	33500	1828660	.453
131.24	177.16	159.17	462.34	292.77	208.63	92.23	33500	1828660	.453
97.98	126.44	108.03	344.90	218.40	141.60	62.60	21800	1188931	.453
70.24	126.44	108.03	344.90	218.40	141.60	62.60	21800	1188931	.453
98.62	126.44	108.03	344.90	218.40	141.60	62.60	21800	1188931	.453
95.65	126.44	108.03	344.90	218.40	141.60	62.60	21800	1188931	.453
88.86	125.41	107.03	342.41	216.82	140.29	62.02	21600	1176860	.453
80.66	125.41	107.03	342.41	216.82	140.29	62.02	21600	1176860	.453
61.94	101.04	83.50	283.82	179.73	109.45	48.38	16400	893207	.453
63.90	99.39	81.96	279.72	177.13	107.43	47.49	16100	875101	.453
57.18	102.14	84.53	286.55	181.45	110.79	48.98	16600	905277	.453
70.37	101.04	83.50	283.82	179.73	109.45	48.38	16400	893207	.453
72.85	101.04	83.50	283.82	179.73	109.45	48.38	16400	893207	.453
211.53	139.93	195.29	245.46	220.91	138.14	63.82	18500	685276	.840
223.60	139.93	195.29	245.46	220.91	138.14	63.82	18500	685276	.840
221.30	139.93	195.29	245.46	220.91	138.14	63.82	18500	685276	.840
203.11	139.93	195.29	245.46	220.91	138.14	63.82	18500	685276	.840
295.18	188.52	274.75	318.29	286.46	194.35	89.78	26800	1000504	.840
282.51	188.52	274.75	318.29	286.46	194.35	89.78	26800	1000504	.840
357.09	188.52	274.75	318.29	286.46	194.35	89.78	26800	1000504	.840
296.61	188.52	274.75	318.29	286.46	194.35	89.78	26800	1000504	.840
108.78	81.42	104.71	153.47	138.13	74.07	34.22	9200	342638	.840
118.30	81.42	104.71	153.47	138.13	74.07	34.22	9200	342638	.840
122.94	83.01	107.16	155.96	140.36	75.80	35.02	9500	351775	.840
109.78	83.01	107.16	155.96	140.36	75.80	35.02	9500	351775	.840
117.58	123.77	79.64	544.43	220.32	141.96	57.22	21200	1268717	.207
128.58	119.68	76.92	526.97	213.25	137.12	55.27	21000	1224312	.207
95.79	123.56	79.15	545.66	220.81	141.08	56.87	20400	1256030	.207
133.43	123.56	79.15	545.66	220.81	141.08	56.87	20400	1256030	.207
104.87	124.05	79.51	547.56	221.58	141.73	57.13	20500	1262374	.207
118.26	124.05	79.51	547.56	221.58	141.73	57.13	20500	1262374	.207
182.98	171.20	115.08	724.64	293.24	205.14	82.68	30800	1903076	.207
163.29	170.75	114.73	722.98	292.57	204.52	82.44	30700	1896733	.207
164.13	171.20	115.08	724.64	293.24	205.14	82.68	30800	1903076	.207
190.54	171.20	115.08	724.64	293.24	205.14	82.68	30800	1903076	.207
173.31	171.20	115.08	724.64	293.24	205.14	82.68	30800	1903076	.207
120.33	171.20	115.08	724.64	293.24	205.14	82.68	30800	1903076	.207
76.88	100.95	62.08	462.12	187.01	110.67	44.61	14400	951538	.207
95.83	100.95	62.08	462.12	187.01	110.67	44.61	14400	951538	.207
87.85	100.95	62.08	462.12	187.01	110.67	44.61	14400	951538	.207
97.28	100.43	61.71	460.06	186.18	110.01	44.34	14300	945194	.207
76.71	100.95	62.08	462.12	187.01	110.67	44.61	14400	951538	.207
103.96	100.95	62.08	462.12	187.01	110.67	44.61	14400	951538	.207
76.78	100.35	61.91	458.09	185.38	110.37	44.49	14800	951538	.207
96.33	100.35	61.91	458.09	185.38	110.37	44.49	14800	951538	.207
227.53	137.53	136.60	374.10	220.58	147.12	64.73	24800	753600	.400
231.99	137.53	136.60	374.10	220.58	147.12	64.73	24800	753600	.400
205.96	135.87	134.64	370.37	218.38	145.00	63.80	24300	741246	.400
190.59	135.87	134.64	370.37	218.38	145.00	63.80	24300	741246	.400
314.83	179.86	186.74	470.55	277.45	201.11	88.48	36200	1069865	.400
300.77	179.86	186.74	470.55	277.45	201.11	88.48	36200	1069865	.400

APPENDIX III

ANALYSIS OF SINGLETON'S DATA

APPENDIX III

Analysis of Singleton's Data

Singleton [22] analyzed his data in terms of a dimensionless mixing coefficient which could be related to $1/N_{Pe}$ by assuming values for gap width and subchannel separation distance. His concentration data were used to evaluate an equivalent Stanton number. The procedure is outlined below.

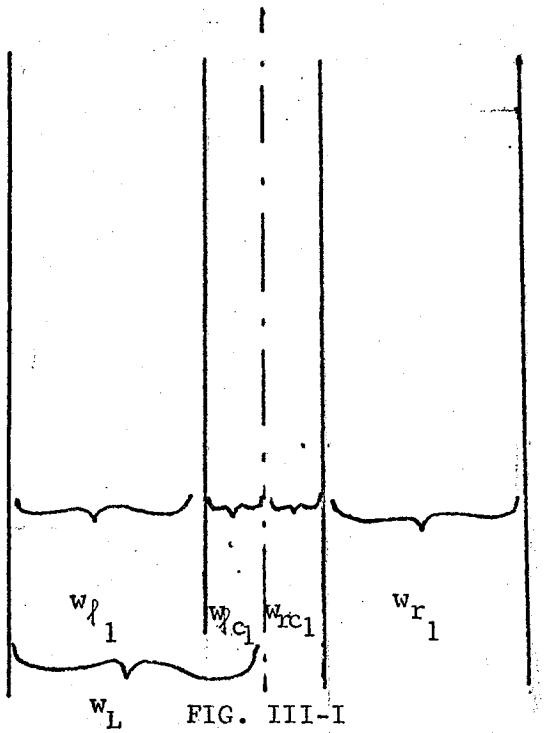

FIG. III-I

Subchannel Flow Designations

$$w_{\ell_1} + w_{c\ell_1} = w_L = w_{\ell_2} + w_{c\ell_2} \tag{A.1}$$

$$w_{r_1} + w_{cr_1} = w_R = w_{r_2} + w_{cr_2} \tag{A.2}$$

$$w_{c\ell_1} = w_{\ell_1} \frac{V_c}{V_1} \frac{A_c}{A_1} \tag{A.3}$$

Denote $\frac{V_c}{V_{\ell}} \frac{A_c}{A_{\ell}} = \frac{V_c}{V_r} \frac{A_c}{A_r}$ by K

i.e. The velocity in the centre channel is greater than in the outer channels.

The inlet concentration in channel one can be written as

$$LC1 = \frac{C_{\ell_1} w_{\ell_1} + C_{\ell c_1} w_{\ell c_1}}{w_L} = \frac{C_{\ell_1} w_{\ell_1} + K C_{\ell c_1} w_{\ell_1}}{w_{\ell_1}(1+K)}$$

$$= \frac{C_{\ell_1} + K C_{\ell c_1}}{1+K} \qquad (A.5)$$

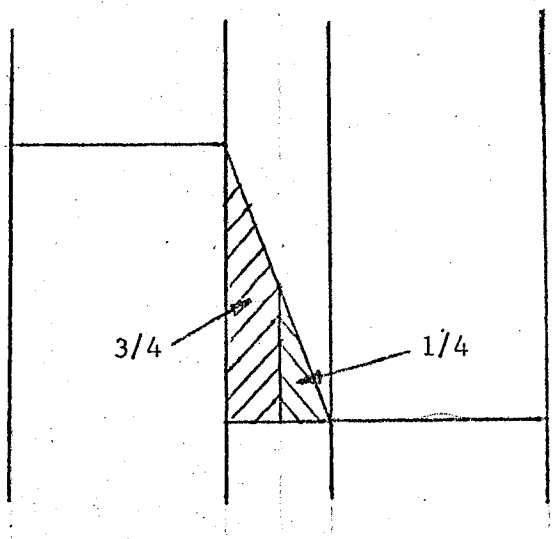

FIG. III-2

Concentration Profile

The concentration gradient can be approximated as linear.

Therefore:

$$C_{\ell c_1} = .75\ C_{c_1}$$

Now the concentration in the left channel at the entrance can be written as:

$$LC1 = \frac{C_{\ell_1} + K\, C_{c_1}\,(.75)}{1+K} \tag{A.6}$$

Similarly,

$$RC1 = \frac{C_{r_1} + K\, C_{c_r}}{1+K} \tag{A.7}$$

$$LC2 = \frac{C_{\ell_2} + K\, C_{c_2}\,(.75)}{1+K} \tag{A.8}$$

$$RC2 = \frac{C_{r_2} + K\, C_{c_2}\,(.25)}{1+K} \tag{A.9}$$

The mixing rate can now be determined from a mass balance.

$$w_{L_1} = w_{L_2} = w_{R_1} = w_{R_2} = w \tag{A.10}$$

$$w\,(LC1) + w^t\,(RC1 + RC2) - w^t\frac{(LC1 + LC2)}{2} = w\,(LC2) \tag{A.11}$$

$$\frac{w^t}{w} = \frac{2(LC1-LC2)}{(LC1+LC2-RC1-RC2)} \tag{A.12}$$

$$N_{st} = \frac{G^t}{G} = \frac{w^t/A^t}{w/A} = \frac{2(LC1-LC2)}{(LC1+LC2-RC1-RC2)}\,(A^t/A_L) \tag{A.13}$$

From a tracer balance

$$LC1+RC1 = LC2+RC2 \tag{A.14}$$

$$LC1-LC2 = RC2-RC1 \tag{A.15}$$

$$N_{st} = \frac{2(RC2-RC1)}{(LC1+LC2-RC1-RC2)}\,(A^t/A_L) \tag{A.16}$$

Using Singletons concentration data a Stanton Number was calculated using Eq. (16). The calculated values are shown in Table III-1.

TABLE III-I

ANALYSIS OF SINGLETON'S DATA

SQUARE FILLERS				ROUND FILLERS			
STANTON NUMBER	REYNOLDS NUMBER	MASS FLUX lb/hr.ft^2	b/d	STANTON NUMBER	REYNOLDS NUMBER	MASS FLUX lb/hr.ft^2	b/d
.003808	33400	1822625	.453	.004484	21200	1268717	.207
.003495	33400	1822625	.453	.005082	21000	1224312	.207
.003820	33500	1828660	.453	.003690	20400	1256030	.207
.003166	33500	1828660	.453	.005140	20400	1256030	.207
.003633	21800	1188931	.453	.004020	20500	1262374	.207
.002606	21800	1188931	.453	.004533	20500	1262374	.207
.003659	21800	1188931	.453	.004652	30800	1903076	.207
.003549	21800	1188931	.453	.004166	30700	1896733	.207
.003331	21600	1176860	.453	.004173	30800	1903076	.207
.003024	21600	1176860	.453	.004845	30800	1903076	.207
.003060	16400	893207	.453	.004406	30800	1903076	.207
.003222	16100	875101	.453	.003059	30800	1903076	.207
.002787	16600	905277	.453	.003909	14400	951538	.207
.003476	16400	893207	.453	.004873	14400	951538	.207
.003598	16400	893207	.453	.004468	14400	951538	.207
.007350	18500	685276	.840	.004980	14300	945194	.207
.007769	18500	685276	.840	.003901	14400	951538	.207
.007689	18500	685276	.840	.005287	14400	951538	.207
.007057	18500	685276	.840	.003904	14800	951538	.207
.007024	26800	1000504	.840	.004899	14800	951538	.207
.006723	26800	1000504	.840	.007548	24800	753600	.400
.008498	26800	1000504	.840	.007696	24800	753600	.400
.007059	26800	1000504	.840	.006946	24300	741246	.400
.007559	9200	342638	.840	.006428	24300	741246	.400
.008221	9200	342638	.840	.007357	36200	1069865	.400
.008321	9500	351775	.840	.007028	36200	1069865	.400
.007430	9500	351775	.840				

APPENDIX IV

APPENDIX IV

The two-phase pressure drop data was compared with the Lockhart-Martinelli model. The results are shown in Table IV - 1.

TABLE IV-1

TWO PHASE PRESSURE DROP DATA

Comparison with Lockhart-Martinelli Correlation

EXPERIMENTAL PRESSURE DROP psi/ft	PREDICTED PRESSURE DROP psi/ft	QUALITY	MASS FLUX $lb/hr.ft^2$	GAS PHASE REYNOLDS NUMBER	LIQUID PHASE REYNOLDS NUMBER	PERCENT DEVIATION
.0912	.0852	.20	97800	36445	2875	- 6.5
.1033	.1008	.20	122249	45556	3678	- 2.3
.1218	.1195	.20	146699	54585	4363	- 1.9
.0724	.0682	.40	73350	54750	1498	- 5.7
.0985	.0936	.40	97800	73222	2156	- 4.9
.1395	.1254	.40	122249	91527	2636	-10
.1839	.1630	.40	146699	108841	3515	-11.4
.0739	.0745	.60	73350	82125	1020	+ 0.9
.1191	.1121	.60	97800	110167	1524	- 5.9
.1716	.1610	.60	122249	136462	1839	- 6.1
.2186	.2167	.60	146699	164002	2343	- 0.9
.0754	.09538	.80	73350	109334	479	+26.5
.1236	.1448	.80	97800	145779	666	+17.1
.1892	.2052	.80	122249	182500	832	+ 8.4
.2721	.2642	.80	146699	217355	1066	- 2.9

APPENDIX V

CALCULATION OF SOLUBILITY OF METHANE IN WATER

APPENDIX V

Calculation of Solubility of Methane in Water

The example used for the following calculation will consider the highest mass flow and lowest quality since this represents the case for the maximum error due to the soluability of methane.

Pressure = 50 psia

$T = 25^{o}C$

Air flow =120 lb/hr

Water flow = 480 lb/hr

Methane concentration .0033 by volume

H (Henry Low Constant [35]) = 4.13×10^{4} $\frac{\text{atm.}}{\text{mole fraction of solute in solution}}$

P_m = partial pressure methane

$= .0033 \times \frac{50}{14.7} = .0112$ atm.

X_m = mole fraction methane in solution

$= \frac{.0112}{4.13 \times 10^{4}} = 2.71 \times 10^{-7}$

Number of moles of water = $\frac{480}{18} = 26.7$ moles/hr

Number of moles of methane dissolved = $2.71 \times 10^{-7} \times 26.7$

$= 7.25 \times 10^{-6}$ moles/hr

Number of moles of methane available = $.0033 \times \frac{120}{29}$

$= .0137$ moles/hr

Percent dissolved = $\frac{7.25 \times 10^{-6}}{1.37 \times 10^{-2}} (100)$

$= .0053\%$

VITA AUCTORIS

1943	Born in Sault Ste. Marie, Ontario
1962	Graduated from St. Mary's High School in Sault Ste. Marie
1966	Graduated from University of Windsor with degree of B.A.Sc. in Chemical Engineering
1966	Accepted into the Graduate School of University of Windsor as a candidate for the degree of M.A.Sc. in Chemical Engineering